SGR 1935+2154 activity in 2016 detected by LOMONOSOV satellite

A.F. Iyudin , V. Bogomolov, A. Bogomolov, M.I. Panasyuk, S.I. Svertilov, I.V. Yashin

Skobeltsyn Institute of Nuclear Physics,
Moscow State University by M.V. Lomonosov

P. Minaev, A. Pozanenko

Space Research Institute, RAS

KW25 Workshop, St.-Petersburg, Russia, 09-13 September, 2019

"LOMONOSOV" SPACE MISSION

Launched April 28, 2016

Scientific objectives:

➢ **Study of transient events at hard x-ray and soft gamma-ray energies (0.01-3.0 MeV)**

➢ **Search and detection of optical transients accompanying GRBs**

➢ **Study of transient events in the Earth atmosphere at UV, X-rays**

➢ **Study of ultra-high energy cosmic rays ➜ synergy with GRBs**

➢ **Earth magnetosphere research**

Lomonosov instruments suite to study GRBs:

- BDRG – gamma spectrometer

- SHOK – wide field optical camera

- UFFO – composed of the coded mask X-ray telescope, and of UV telescope
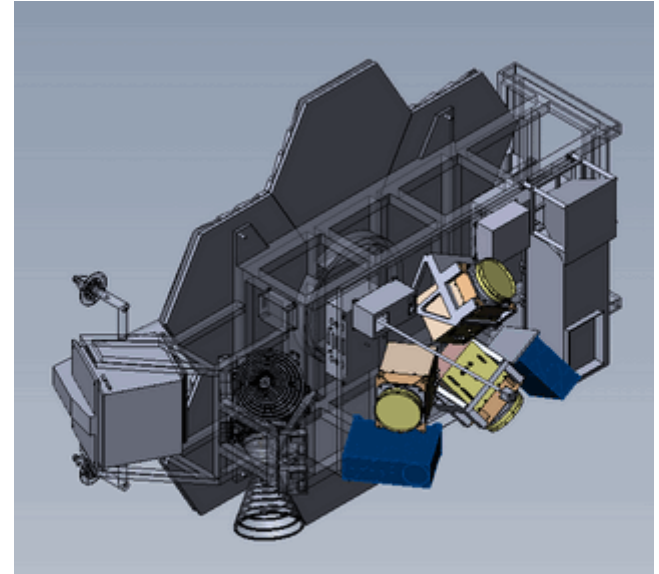

Parameters of mission:
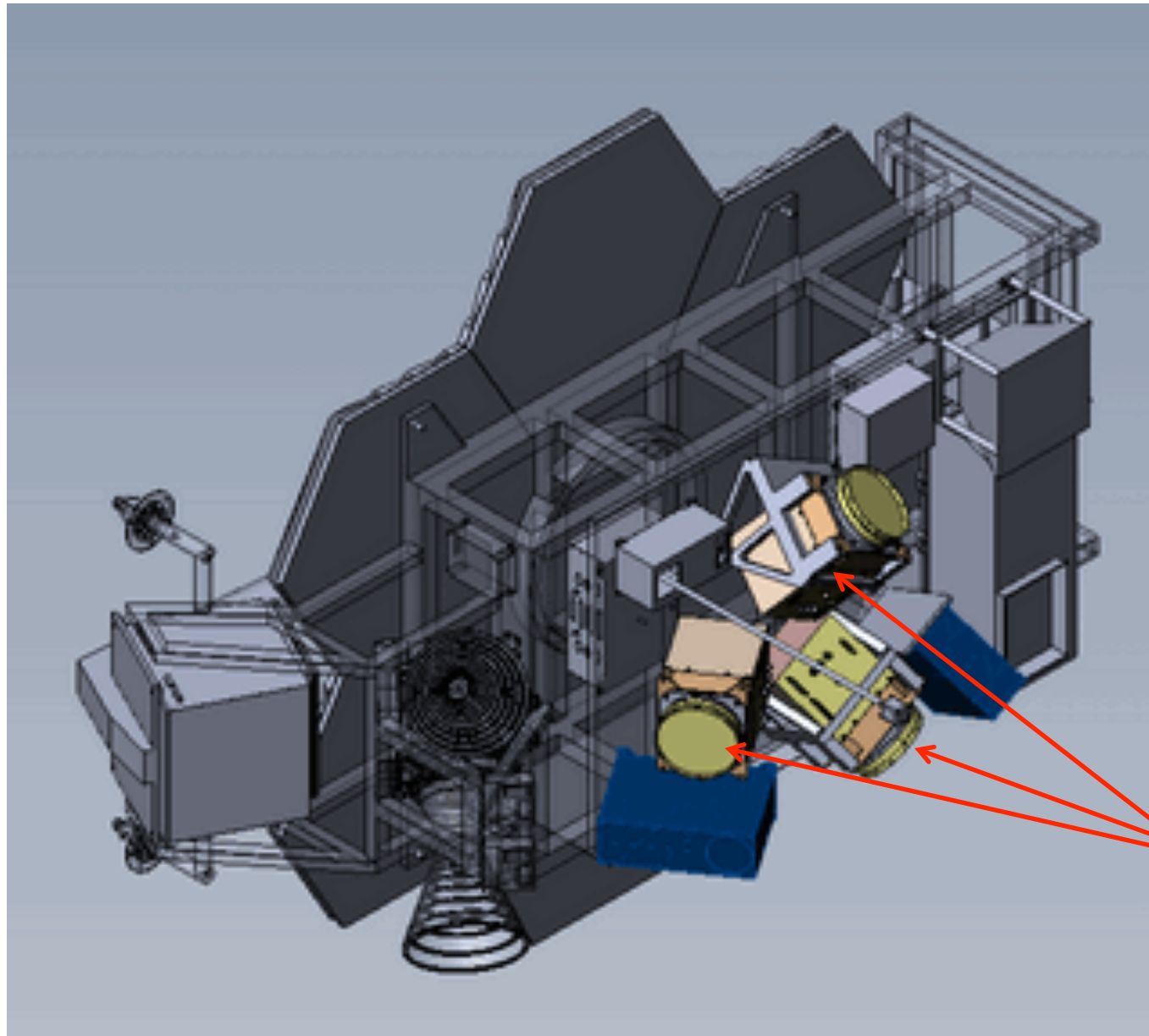
Orbit: 520 km, solar-synchronous

Mass: Spacecraft ~500 kg; Scientific payload ~120kg
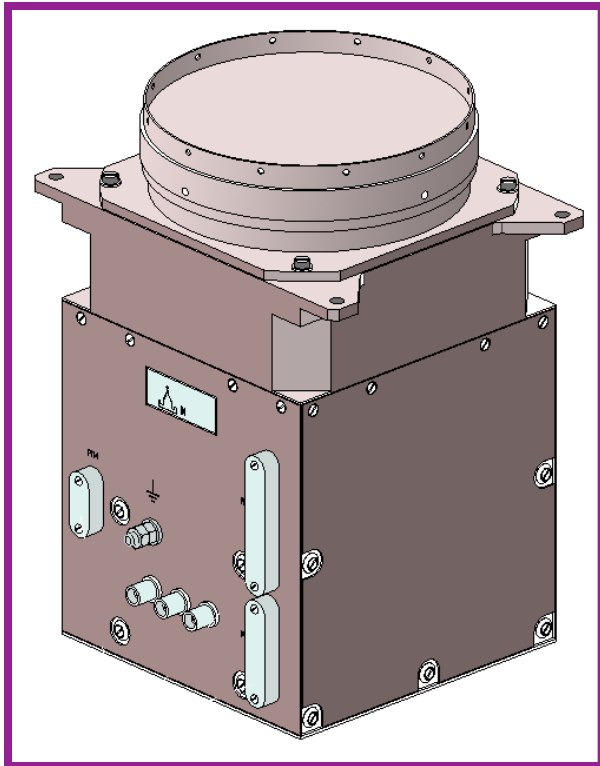
Total power ~ 300W

Launch time – April 2016

Complex of instruments to study GRB:

BDRG

BDRG on-board "Lomonosov"

1. Produce GRB trigger for SHOK
2. Spectral measurements and timing of transients at hard x-ray and gamma energies
3. Estimation of GRB coordinates
3. X-ray and gamma-ray all-sky monitoring

Parameter, units	Value
Energy range, MeV	0.01–3.0
Effective area (for three detectors), cm^2	~ 360
Time resolution, ms	1 (for the burst mode)
Mass (for one detector module), kg	5.5
Information capacity, MByte/day	~ 500
Field of view, sr	2
Field of effective source location, sr	2
Sensitivity to the burst detection, erg/cm^2	$\sim 10^{-7}$
Accuracy of burst source location	~ 2–$4°$ (for brightest events)
Expected number of detected bursts per year	~ 100
Power consumption, W	22.5

BDRG detector unit

Detector consists of optically coupled thin (3mm) NaI(Tl) with considerably thicker (17mm) CsI(Tl) crystal.

Thickness of NaI(Tl) is optimized for soft part of energy range. CsI(Tl) plays a role of active shield for the soft radiation, and is main detector for the hard one.

Energy ranges are 0.01-0.5 MeV for NaI(Tl) and 0.05-3 MeV for CsI(Tl) crystals, accordingly.
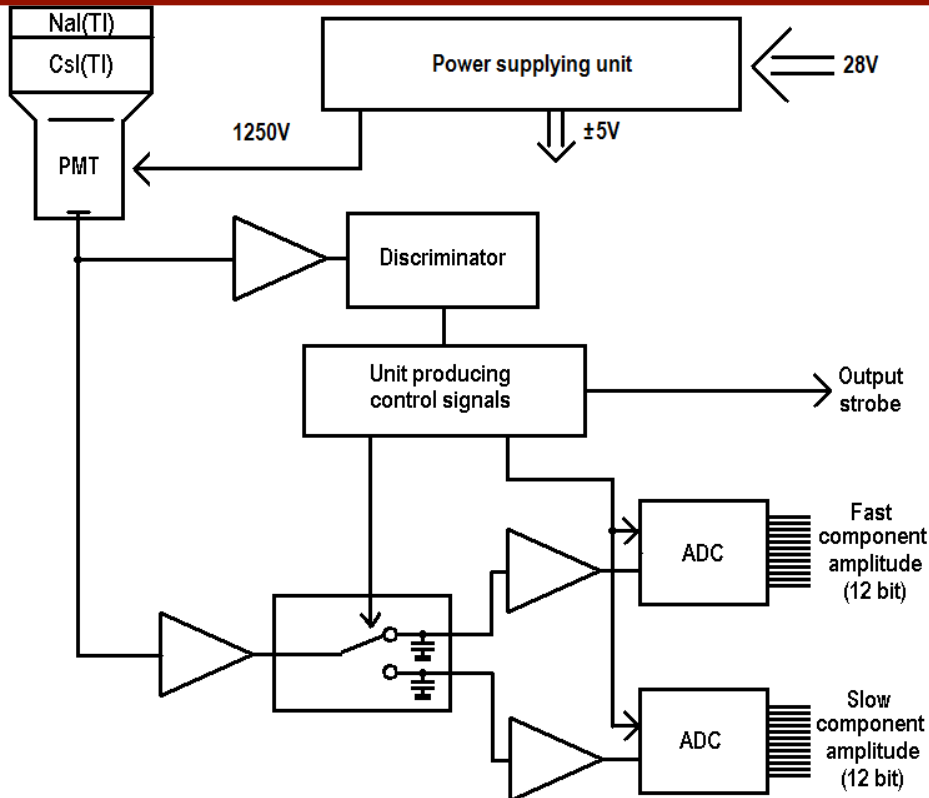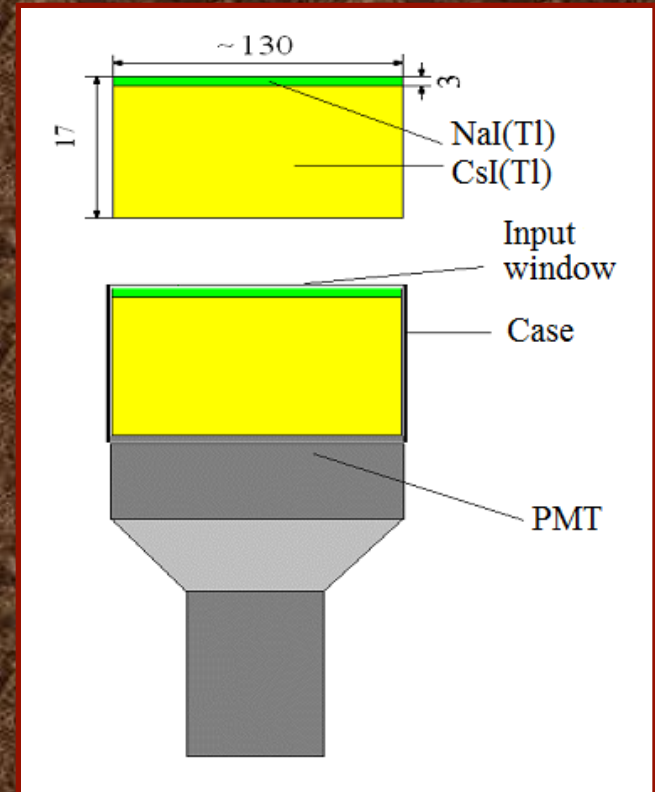
Parallel coded amplitude of PMT signal is integrated for the first ~600ns and during the next ~3μs is read-out by BDRG electronics (BE BDRG) together with request "output strobe". Data frames, GRB trigger, etc are formed by the BE BDRG
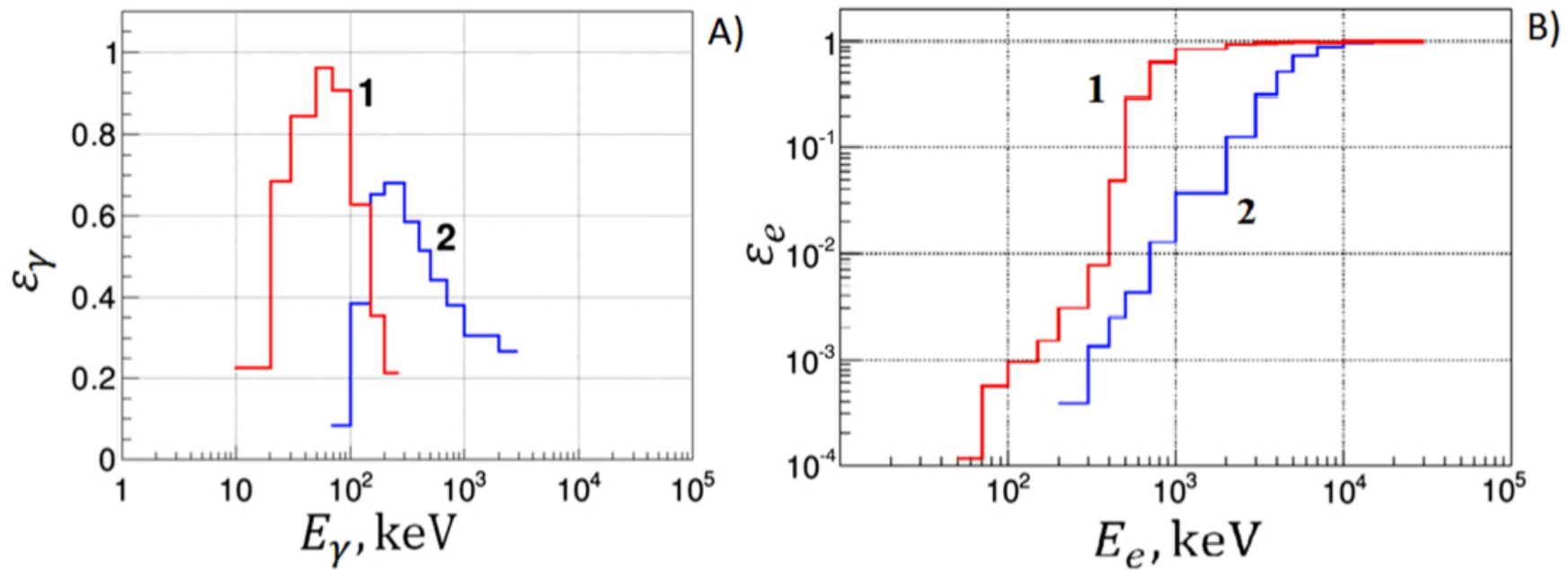
Fig. 8 (**A**) Efficiency of gamma quantum detection in NaI(Tl) (1) and CsI(Tl) (2) crystals of BDRG. (**B**) Electron detection efficiency in NaI(Tl) (1) and CsI(Tl) (2) crystals of BDRG detector units

NaI(Tl)	CsI(Tl)
10–20 keV	0.03–0.06 MeV
20–35 keV	0.06–0.1 MeV
35–60 keV	0.1–0.18 MeV
60–100 keV	0.18–0.3 MeV
180–300 keV	0.3–0.45 MeV
180–300 keV	0.45–0.8 MeV
300–450 keV	0.8–1.6 MeV
450–650 keV	1.6–3.0 MeV

Svertilov+2018

Examples of BDRG data use for GRB160720 analysis

Count rate of NaI(Tl) part of the BDRG-2 detector at 20-170 keV for GRB160720

BDRG-2 spectrum for GRB160720 using data of both scintillators NaI(Tl) and CsI(Tl)
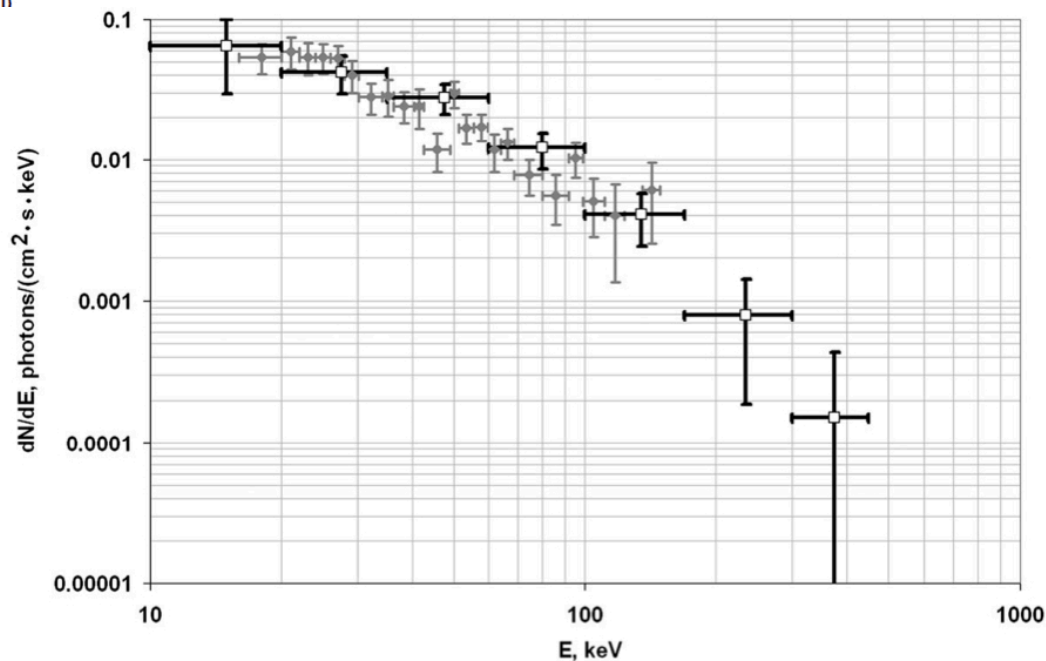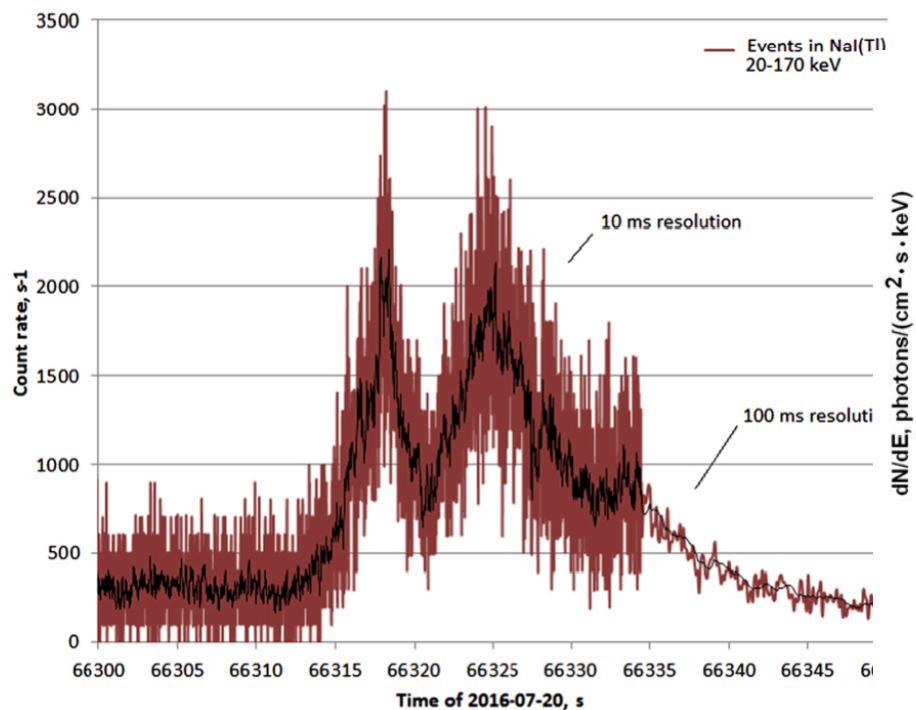

Fig. 17 The energy spectrum of GRB161017A measured by Lomonosov/BDRG (*empty squares*) and Swift/BAT (*light-grey filled points*). The Swift/BAT data were downloaded from Swift Burst Analyser (Barthelmy et al. 2005) and processed according "BAT Data Analysis Guidelines" (http://swift.gsfc.nasa.gov/

MAGNETARS and their general properties

- X-ray pulsars with $L_x \sim 10^{31}$ - 10^{36} erg s^{-1}
- X-ray luminosity generally larger than the rotational energy loss rate
- soft and hard X-ray emission (0.5-200 keV); thermal + non-thermal spectral components
- rotating with $P \sim 0.3$ - 12 s
- magnetic fields of $\sim 10^{13}$ - 10^{15} Gauss **
- flaring activity in X-ray/gamma-ray energy range (0.01 - 10^2 s; $L_x \sim 10^{38}$ - 10^{46} erg s^{-1})
- large outbursts with $E \sim 10^{40}$ - 10^{43} erg (time scale months-years)
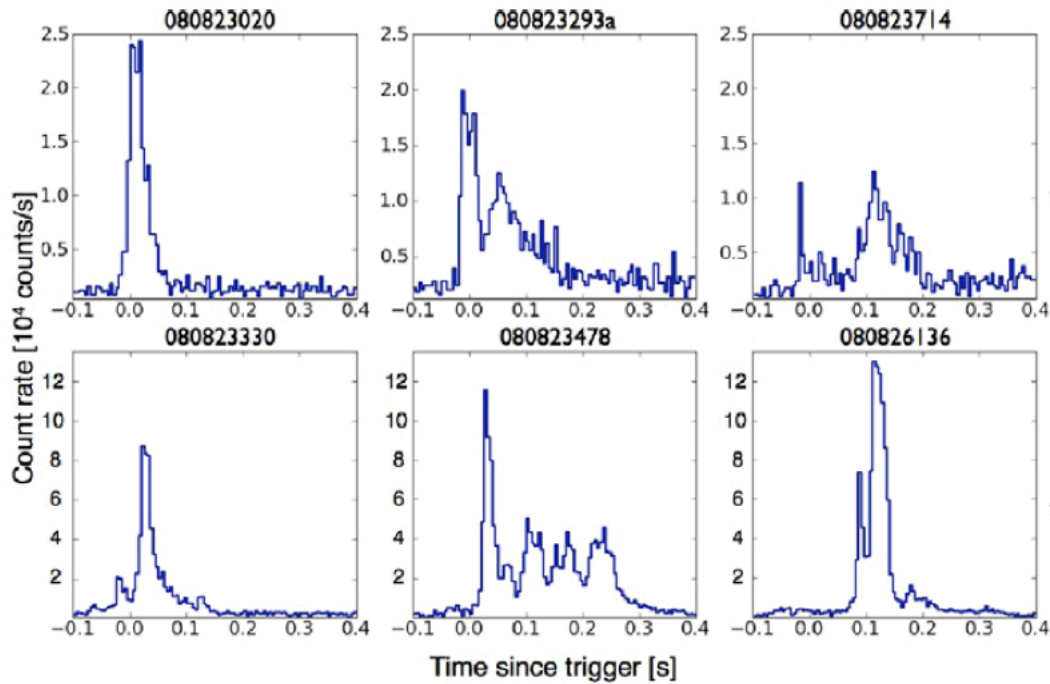- transient radio emission detected in 4 cases

Ref.: Turolla et al. 2015; Kaspi & Beloborodov 2017

** See different interpretation by G.S. Bisnovatyj-Kogan (2016) in the "Handbook of Supernovae", Springer, Alsabti and Murdin (eds.)
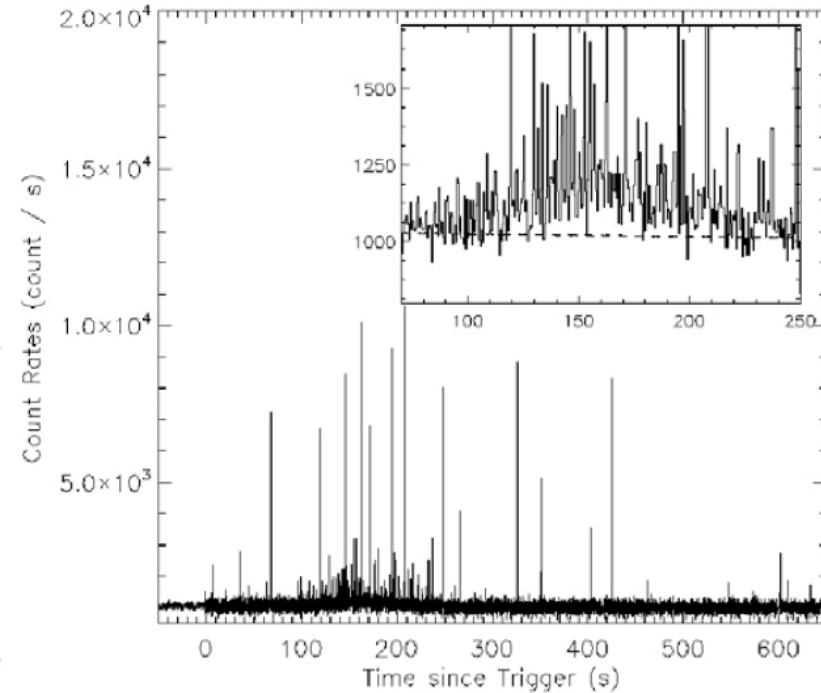
Magnetar's flaring activity

Short bursts (timescale: sec)
- duration ~0.01-1s
- L x ~10^{39} -10^{41} erg s^{-1}
- soft γ-rays thermal spectra (kT ~ 10-40 keV)

Short-bursts forest (timescale: sec/min)


Kaneko+10 (1E1547.0-…)

Huppenkothen+13 (SGR 0501+)

Magnetar's flaring activity

Intermediate bursts

- duration 1-40 s
- peak $\sim 10^{41} - 10^{43}$ erg s^{-1}
- abrupt on-set
- soft γ-rays thermal spectra

Giant Flares

- very rare events (only 3 observed)
- L x > 3×10^{44} erg s^{-1}
- initial peak lasting <1 s with a hard spectrum
- ringing tail that can last > 500s, with softer spectrum and showing the NS spin pulsations

Hurley+99 (SGR1900+14)
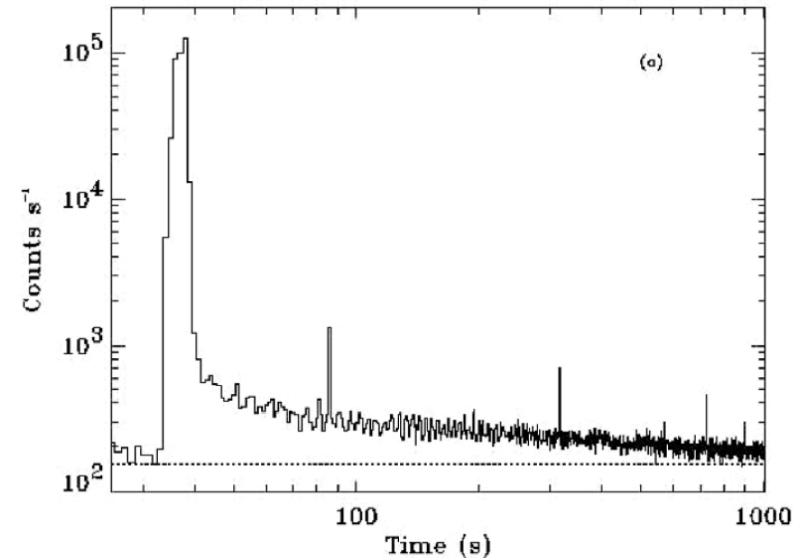
Ibrahim+(2001)
(SGR1900+14)
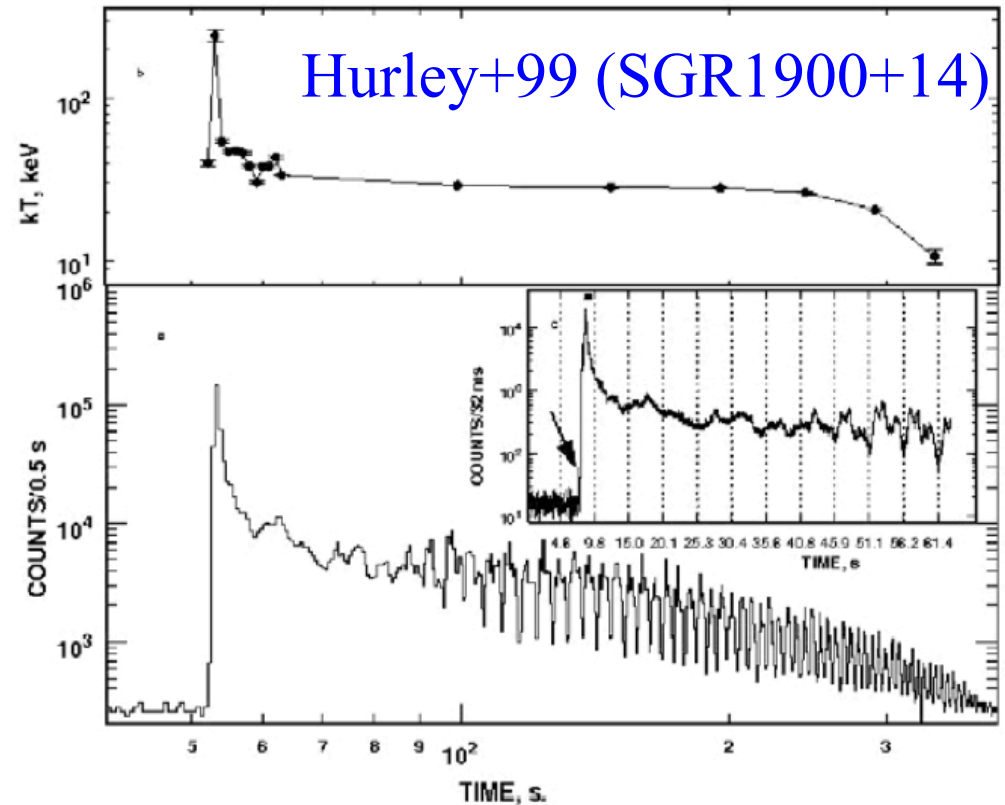
Outburst activity: mechanisms

Internal source of heat
Magnetic stresses in localised parts of the crust

Plastic flows convert magnetic energy into heat

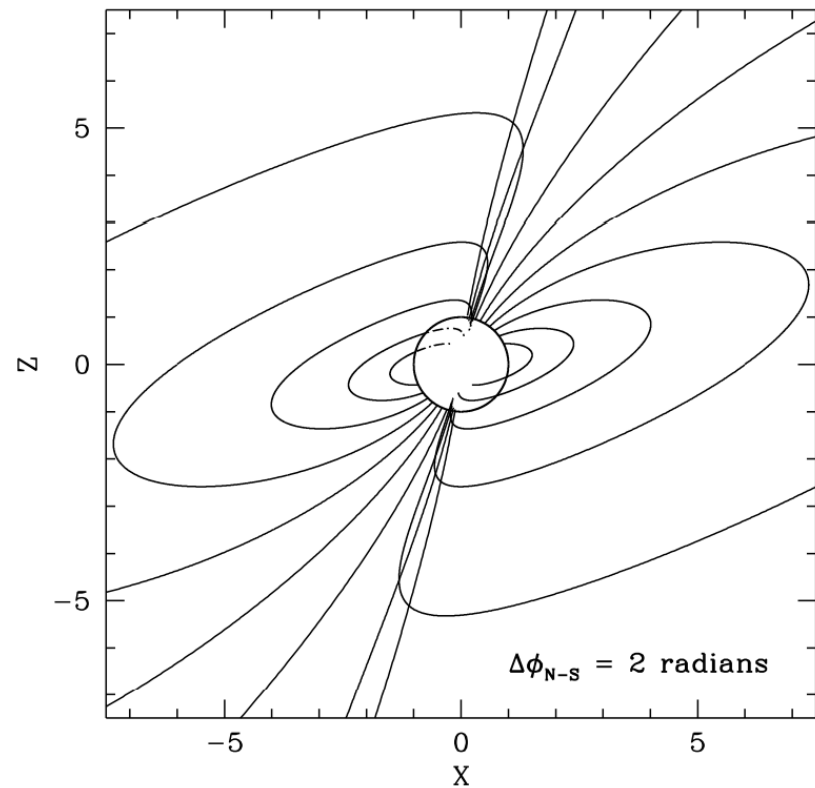Heat conducted up and radiated

External source of heat

Crustal displacements twist up the external B-field.

Returning currents hit the surface

The bundle dissipates as the energy
supply from the star interior decreases

Both processes are likely at work.
Turolla et al. 2015; Kaspi & Beloborodov 2017

$\Delta\phi_{N-S} = 2$ radians

(Thompson&Duncan 1995;
Thompson+Beloborodov 2005;
Beloborodov+Thompson 2007;
Beloborodov 2009, etc..)

Outburst activity: mechanisms

Internal source of heat
Magnetic stresses in localised parts of the crust

Plastic flows convert magnetic energy into heat

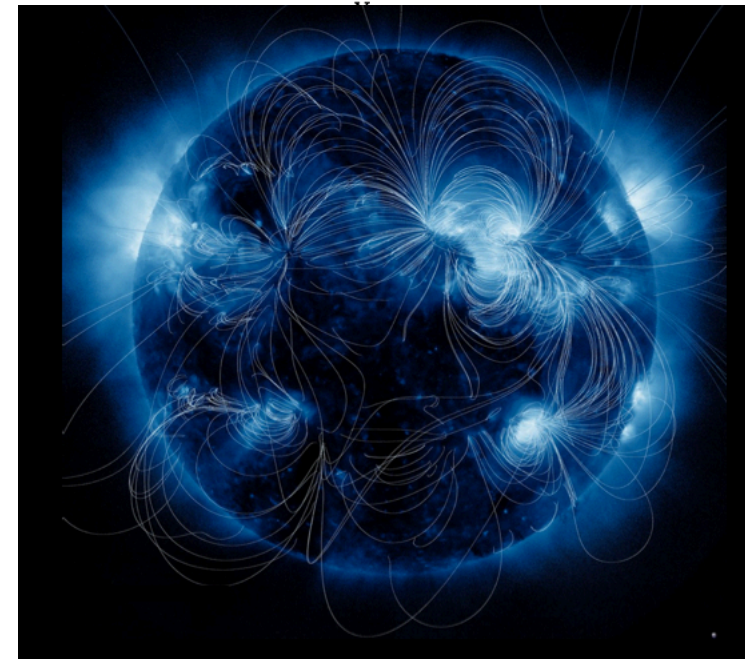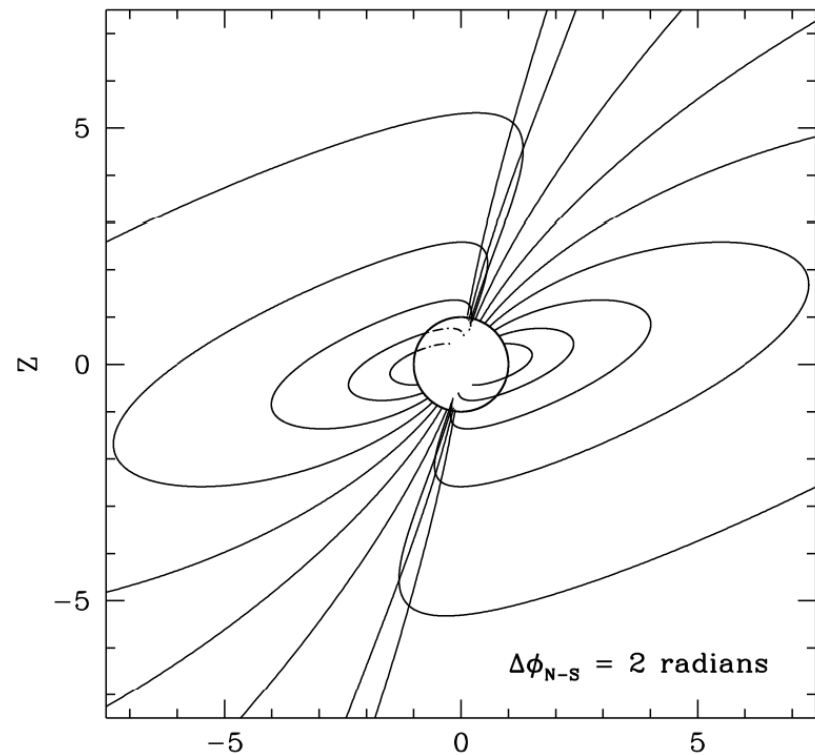Heat conducted up and radiated

External source of heat

Crustal displacements twist up the external B-field.

Returning currents hit the surface

The bundle dissipates as the energy
supply from the star interior decreases

Both processes are likely at work.
Turolla et al. 2015; Kaspi & Beloborodov 2017

$\Delta\phi_{N-S} = 2$ radians

Outburst activity: mechanisms

Internal source of heat
Magnetic stresses in localised parts of the crust

Plastic flows convert magnetic energy into heat

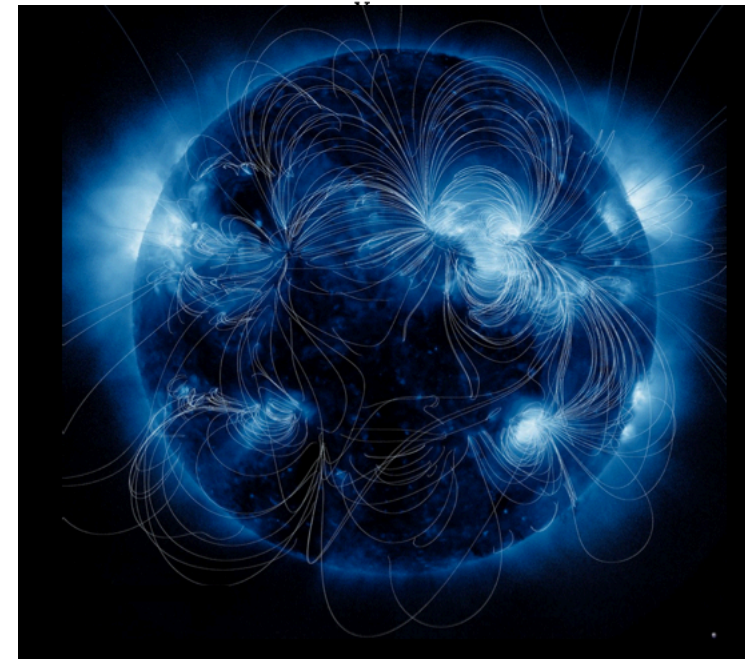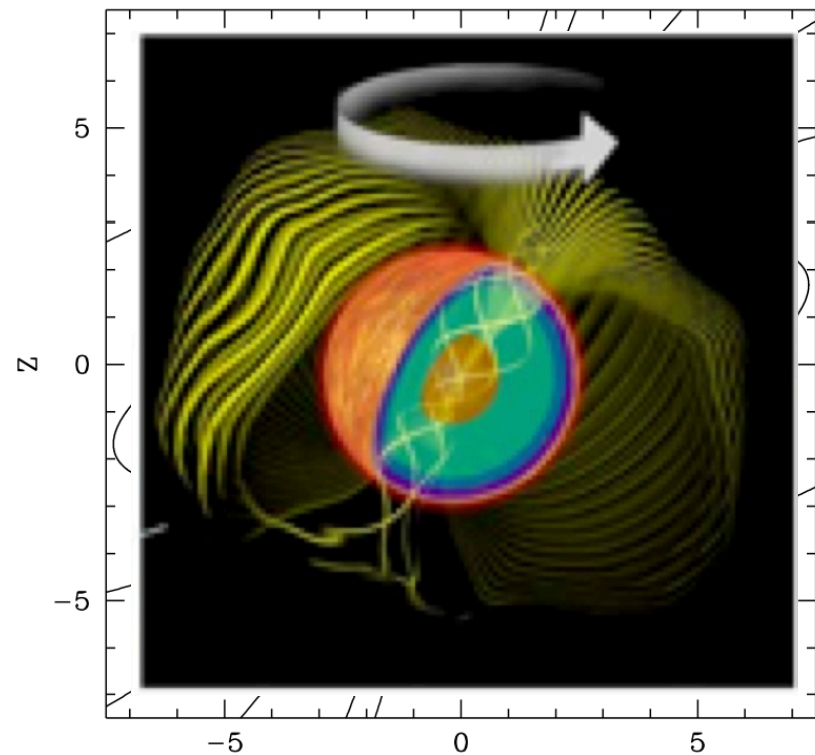Heat conducted up and radiated

External source of heat

Crustal displacements twist up the external B-field.

Returning currents hit the surface

The bundle dissipates as the energy
supply from the star interior decreases

Both processes are likely at work.
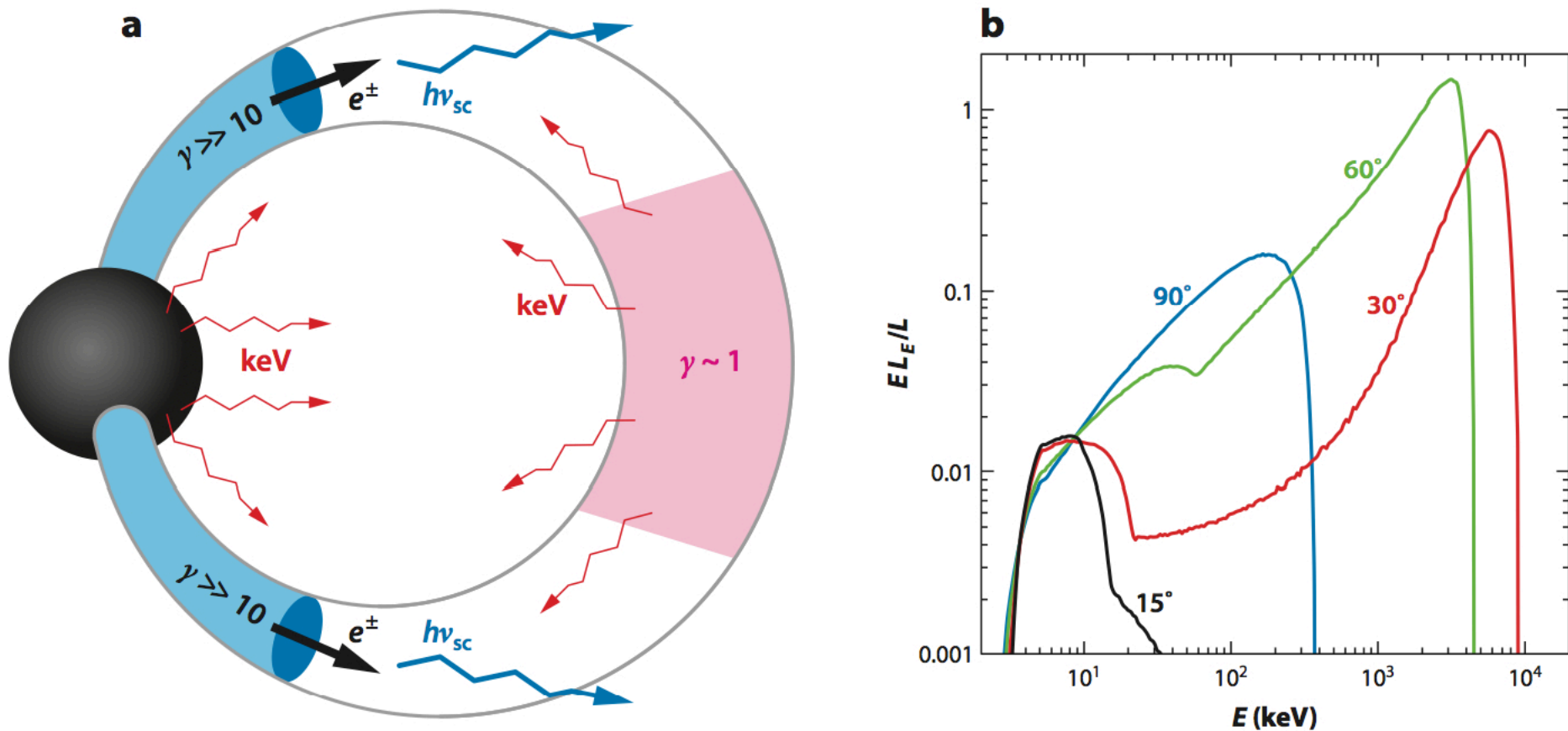Turolla et al. 2015; Kaspi & Beloborodov 2017

Figure 8

(*a*) A magnetic loop in the j-bundle. Relativistic particles are assumed to be injected near the star (*black sphere*), and a large $e^{\pm}$ multiplicity $\mathcal{M} \sim 100$ develops in the adiabatic zone $B > 10^{13}$ G (*blue shading*). The outer part of the loop is in the radiative zone; here the resonantly scattered photons of energy $h\nu_{sc} \sim 1\, B_{13}^2$ MeV escape and form the observed hard X-ray spectrum. The outflow decelerates and eventually annihilates at the top of the loop (*pink shading*); here it becomes opaque to the thermal keV photons flowing from the star. Photons reflected from the pink region have the best chance to be scattered by the relativistic outflow in the lower parts of the loop and control its deceleration. The footprint of the j-bundle is heated by the relativistic backflow from the discharge region; in an axisymmetric model it forms a hot ring on the stellar surface. (*b*) Radiation spectrum from the j-bundle viewed at four different angles with respect to the magnetic dipole axis. Adapted from Beloborodov (2013a) with permission.
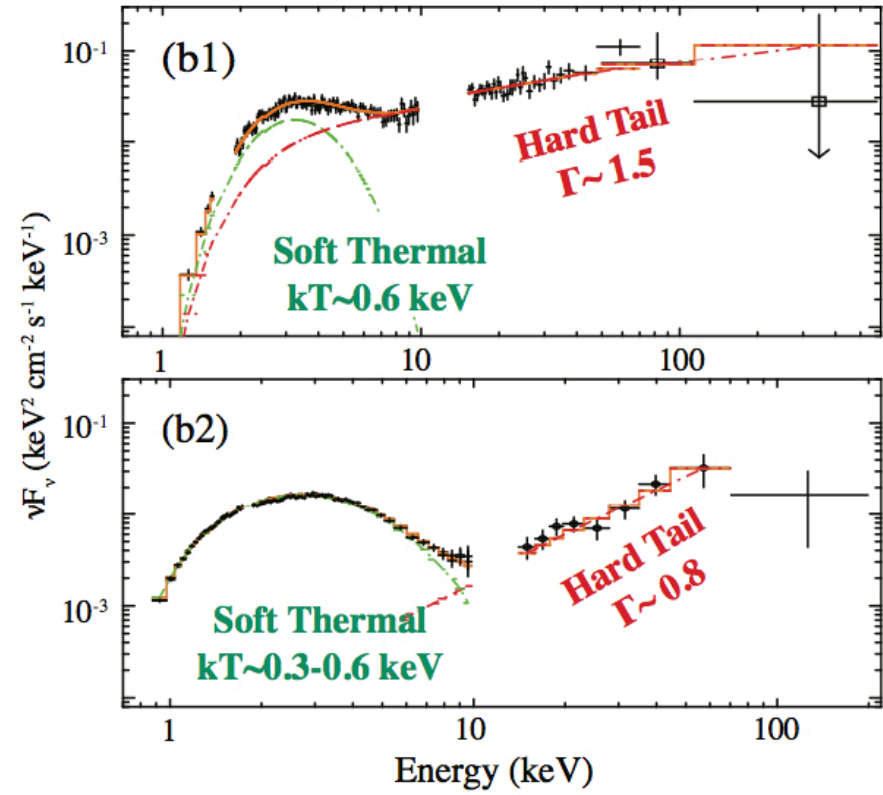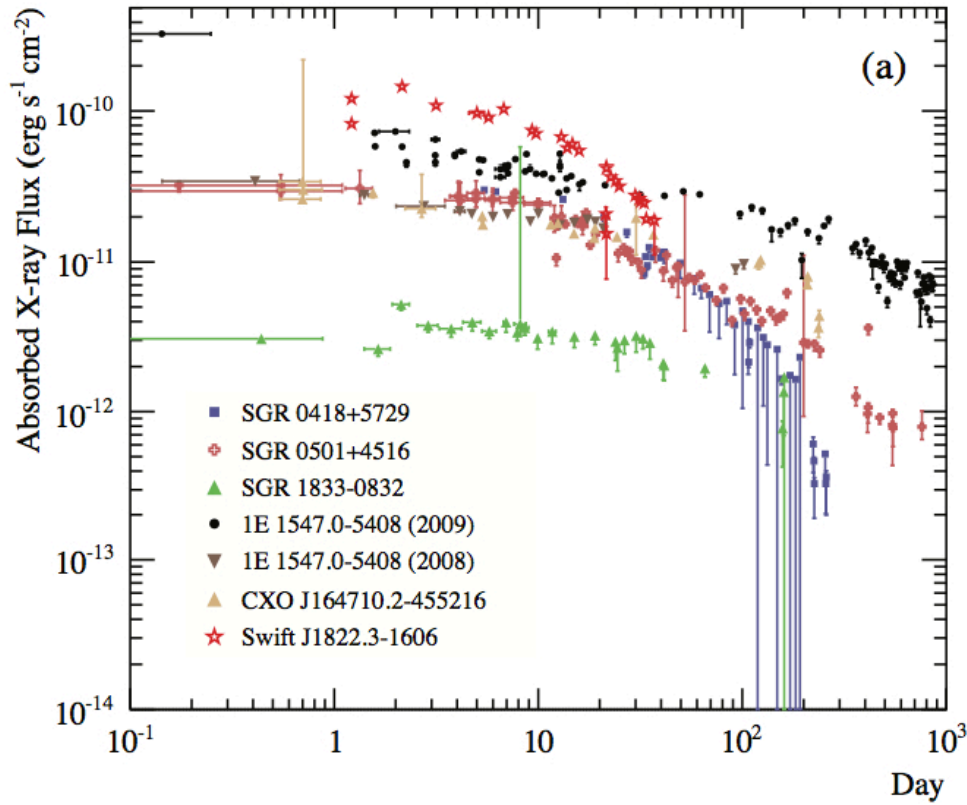
Kaspi & Beloborodov @ ARA&A (2017)

Figure 24: (a) Absorbed 2-10 keV X-ray fluxes of transient magnetars monitored with Swift/XRT, *RXTE*/PCA, and *Suzaku*/XIS. The time onset corresponds to the first detection of magnetar short bursts from these sources, mainly detected with *Swift*/BAT. (b) *Suzaku* spectra during recent two transient activities of 1E 1547.0−5408 (b1) and SGR 0501+4516 (b2) (Enoto et al., 2010c,d).

Astro-H-WP: Kitamoto, Enoto, Safi-Harb et al., arXiv1412.1165v1

Lomonosov detections of SGR 1935+2154

A new member of the growing family of magnetars, i.e., SGR 1935+2154 was discovered by Swift on 2014, July 05 via detection of persistent short duration bursts of X-rays.
The source was active during 2015-2016 years that is well documented by Swift, GBM (Fermi), RHESSI and Konus-Wind detections.
Lomonosov has joined the study of the new magnetar activity by detecting 14 flashes from this SGR 1935+2154 during 2016 by BDRG-1, 2, 3 detectors flying on-board of Lomonosov satellite.

SRG 1935+2154 flares of 2016 detected by BDRG

The event number	1	2	3	4	5	6	7	8	9	10	11	12	13	14
Date	18.06.16	20.06.16	23.06.16	23.06.16	23.06.16	23.06.16	23.06.16	23.06.16	23.06.16	23.06.16	23.06.16	23.06.16	26.06.16	17.07.16
Time Start	20:27:24	15:16:34	15:16:09	15:16:27	16:49:57	17:07:36	17:21:05	20:06:37	20:13:45	21:20:45	21:23:35	22:41:58	13:54:29	09:49:30
Time End	20:27:24	15:16:34	15:16:09	15:16:27	16:49:57	17:07:36	17:21:05	20:06:37	20:13:45	21:20:45	21:23:35	22:41:58	13:54:30	09:49:30
Total duration, s	0.1	0.207	0.1	0.3	0.3	0.2	0.2	0.03	0.2	0.5	0.1	0.1	0.8	0.1
Best time resolution available, s	0.1	**0.001**	0.1	0.1	0.1	0.1	0.1	**0.001**	0.1	0.1	0.1	0.1	0.1	0.1
minimal channel, keV	10-20	10-20	10-20	10-20	10-20	10-20	10-20	10-20	10-20	10-20	10-20	10-20	10-20	10-20
Maximal channel, keV	60-100	60-100	35-60	35-60	60-100	60-100	100-170	35-60	60-100	60-100	60-100	60-100	60-100	60-100
Best illuminated BDRG box	BDRG2	BDRG1	BDRG1	BDRG1	BDRG2	BDRG1	BDRG1	BDRG1	BDRG1	BDRG2	BDRG2	BDRG3	BDRG1	BDRG1
Detectors*	11X	10X	110	110	110	100	100	100	100	110	110	X10	1X1	101
L	>2	<2	<2	<2	<2	<2	>2	<2	<2	>2	>2	<2	<2	>2
Angle(BDRG1), degrees	65	17,5	40,5	40	42	24	56,5	23	20	73	66	100	47	70
Angle(BDRG2), degrees	32	99	50	51	49	108	147	75	99	27	28	57	42,5	157
Angle(BDRG3), degrees	108	76	84	83	85	75	96	74	73	111	103	146	85	79
Count rate /0.1s 10-20keV	280	566	22	58	130	230	133	80	122	228	170	25	452	58
Count rate /0.1s 20-35keV	390	451	17	51	140	220	205	50	110	274	236	60	378	84
Count rate /0.1s 35-60 reV	200	238	9	25	90	90	190	30	40	156	94	35	227	32
count rate /0.1s 60-100 keV	40	67.1	0	0	15	17	101	0	18	49.6	35.7	10	66.3	0
count rate /0.1s 100-170 keV	0	0	0	0	0	0	12	0	0	0	0	0	0	0
count rate /0.1s total	910	1322.1	48	134	375	557	641	160	290	707.6	535.7	130	1123.3	174
(20-35)/(60-100) in peak	9.75	6.72	-	-	9.33	12.94	2.03	-	6.11	5.52	6.61	6.00	5.70	-
Other experiments	Fermi	Fermi, Konus-WIND	Fermi	Fermi	Fermi	-	Konus-WIND	Fermi	-	Konus-WIND	Fermi	Fermi	Fermi, Konus-WIND, Swift	-

* Three symbols indicate work of BDRG-1, BDRG-2 and BDRG-3 in time of SGR flare,

where: 1- indicate SRG burst detection; 0 – no burst observed; X – no data from this unit.

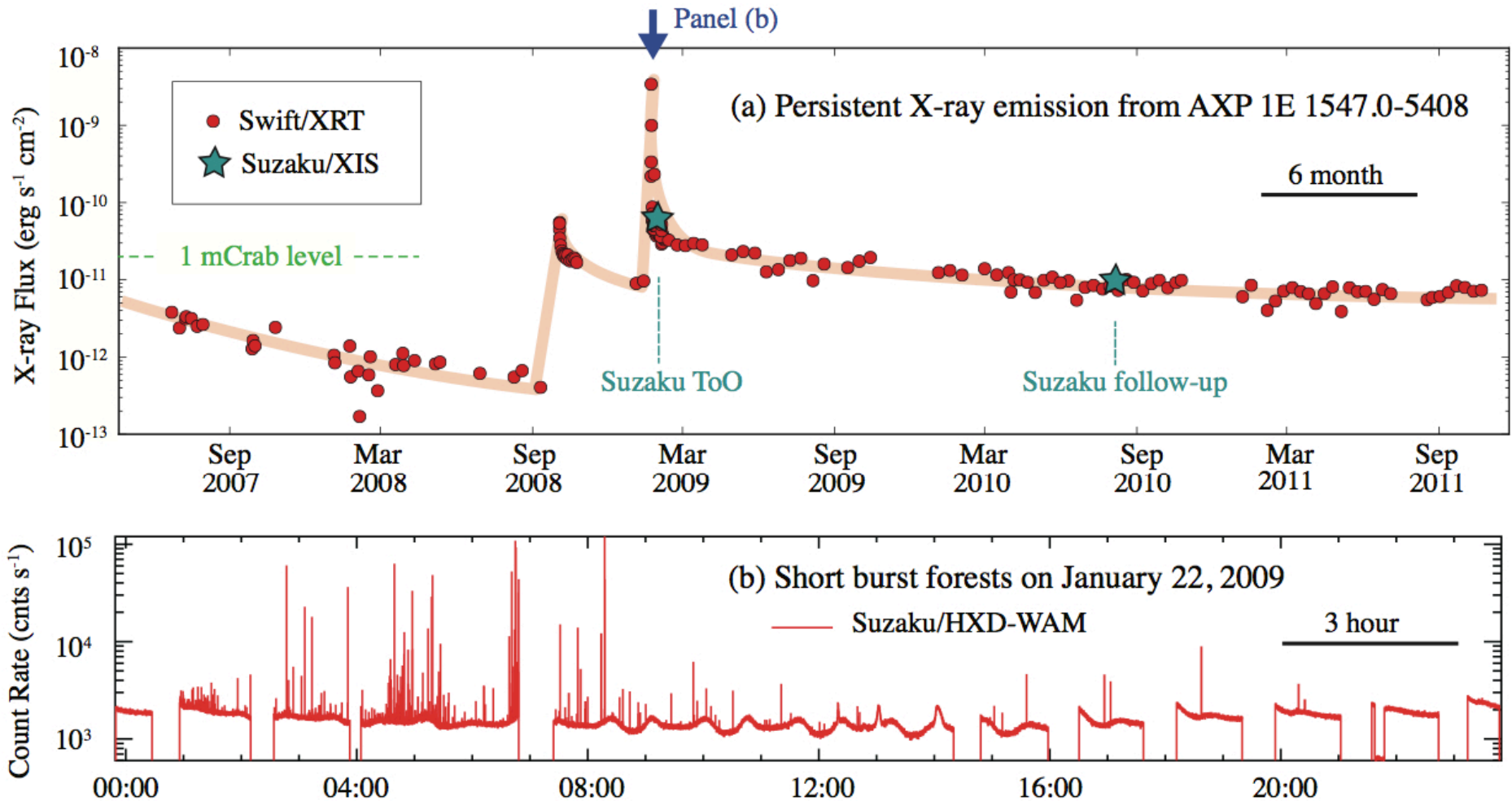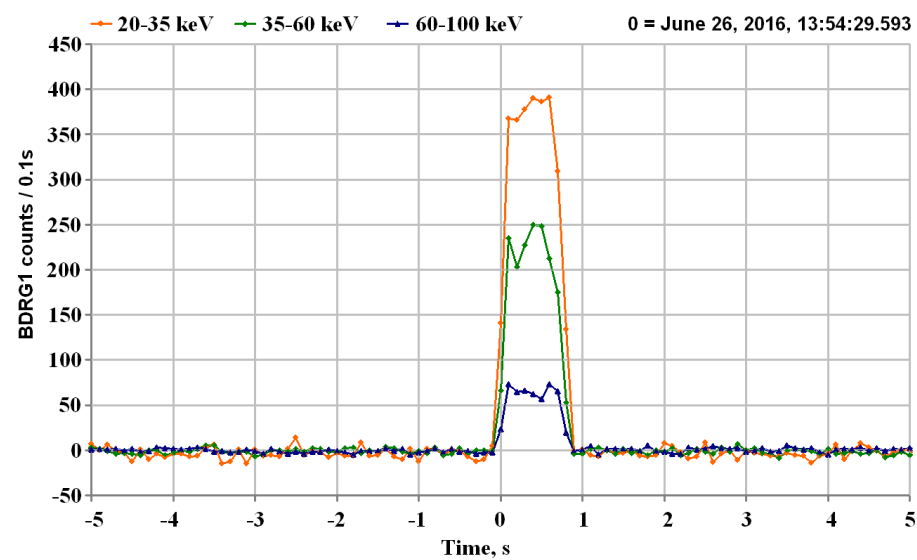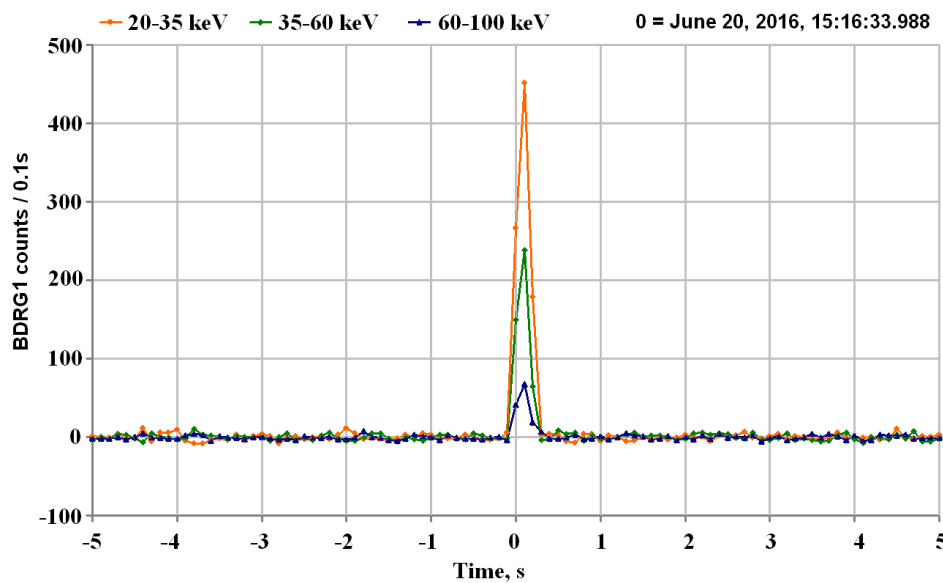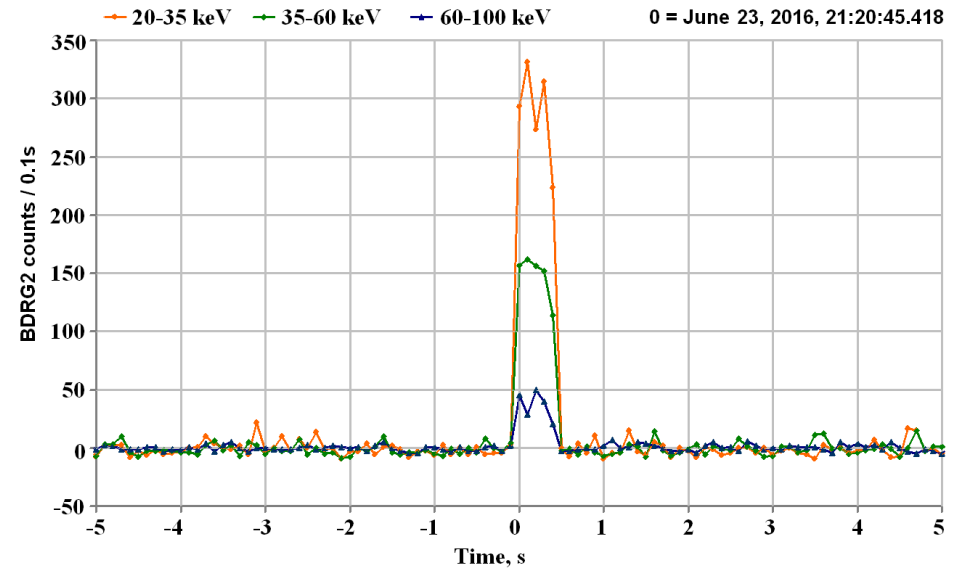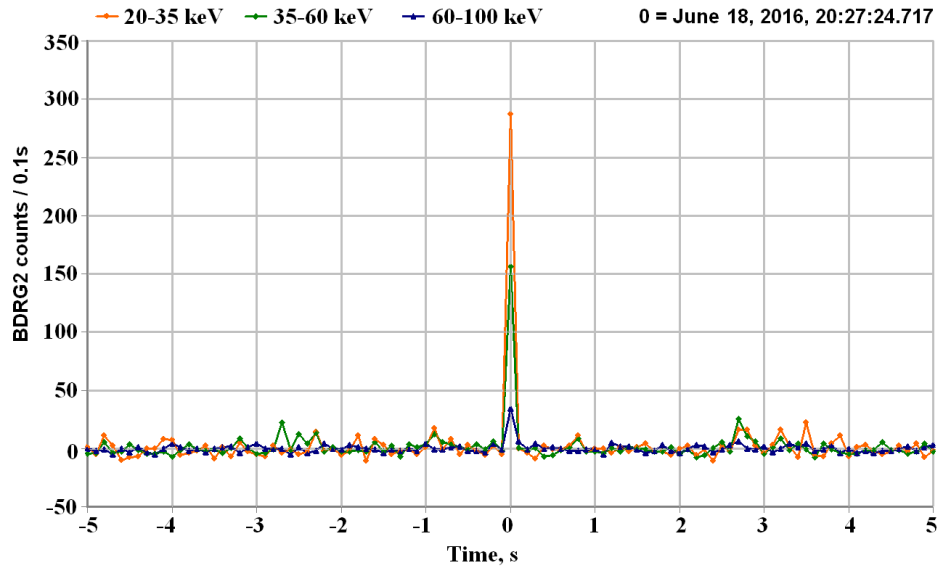# Magnetar's persistent emission and short bursts (forest)

Figure 23: (a) A long-term SXC monitoring of AXP 1E 1547.0−5408 with *Swift*/XRT, with the absorbed 2-10 keV X-ray flux shown. Two *Suzaku* observations are also shown in green stars (Enoto et al., 2010c). (b) Short burst forests from this source recorded by *Suzaku*/HXD-WAM on January 22, 2009, indicated by a blue arrow in panel (a).

Some light curves for different bursts of SGR1935+2154 from the table

Comparison of BDRG count-rates with that of GBM detected bursts for SRG1935+2154

Israel+(2016)
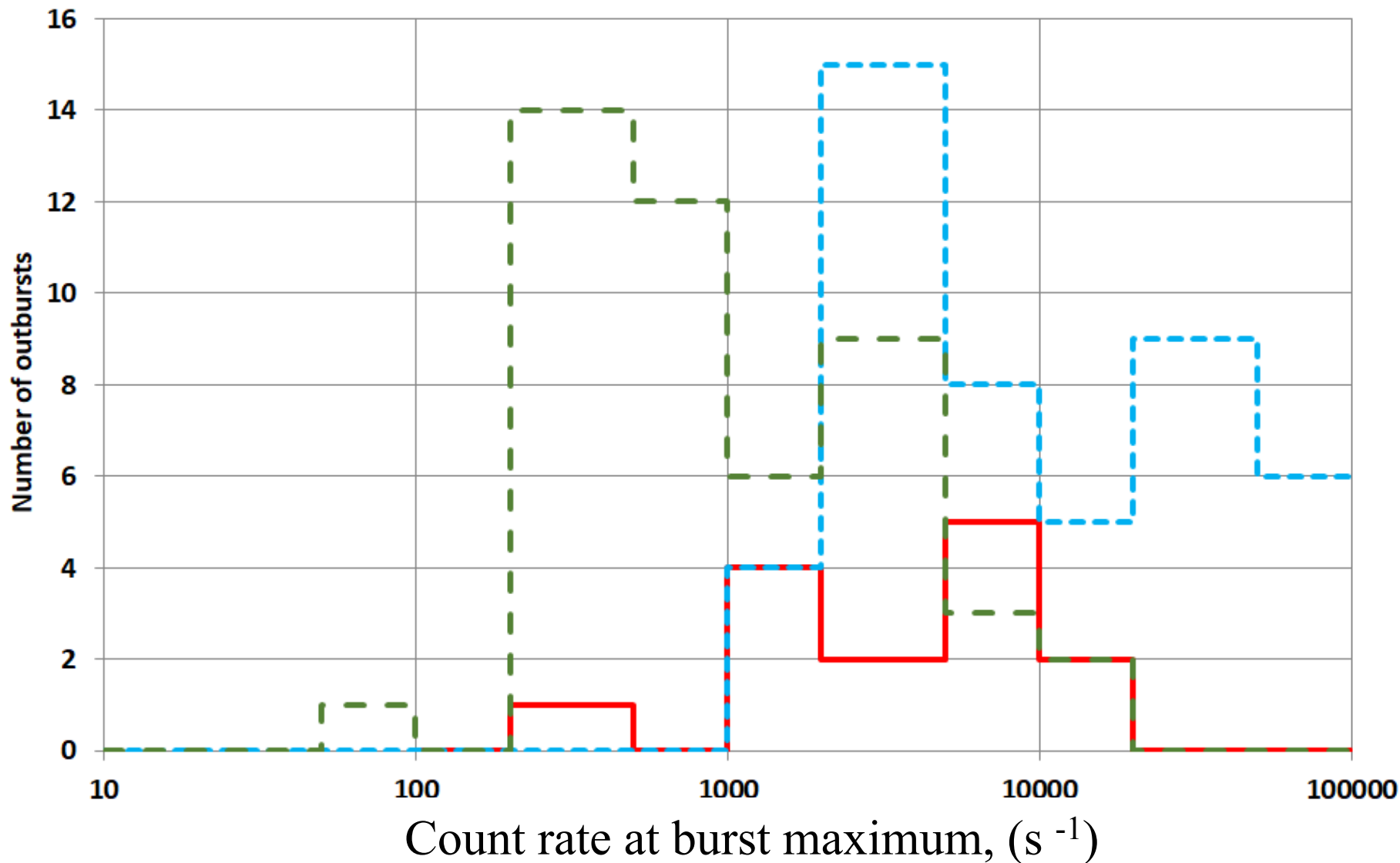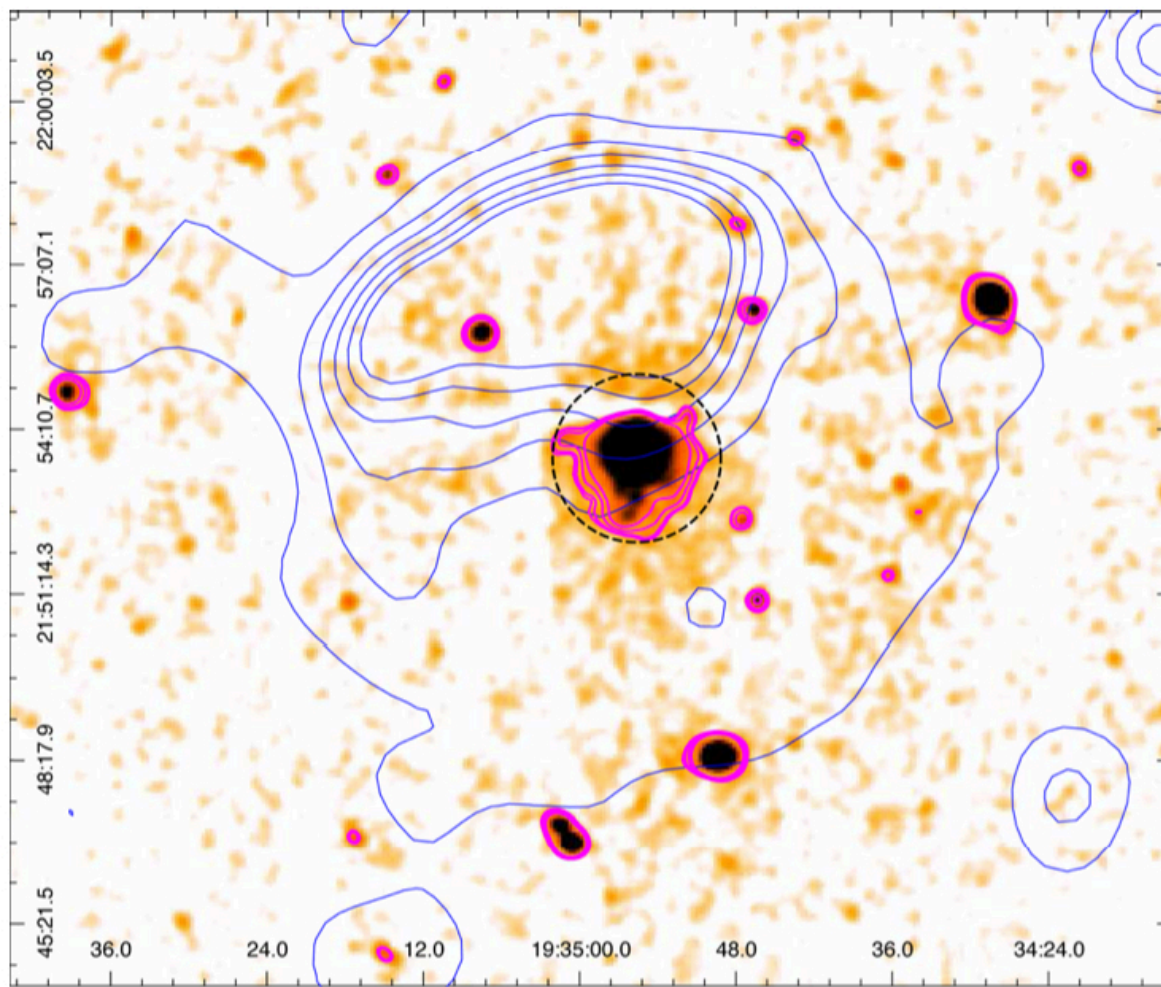
Figure 1. Top: 98 ks-long *XMM–Newton* PN image of the region around SGR J1935+2154; the 1.4 GHz radio map of SNR G57.2+0.8 is also shown (blue contours from the VLA Galactic Plane Survey; Stil et al. 2006, upper image). The *XMM–Newton* image has been smoothed with a Gaussian function with a radius of 4 arcsec and magenta contours are displayed in order to emphasize the extended emission around SGR J1935+2154. The black dashed circle marks a distance of 90 arcsec from the SGR J1935+2154 position. Bottom: 2014 and 2015 *XMM–Newton* and *Chandra* surface brightness

Spectrum of BDRG-1 (NaI) for 2016.06.20 15:16:34 event
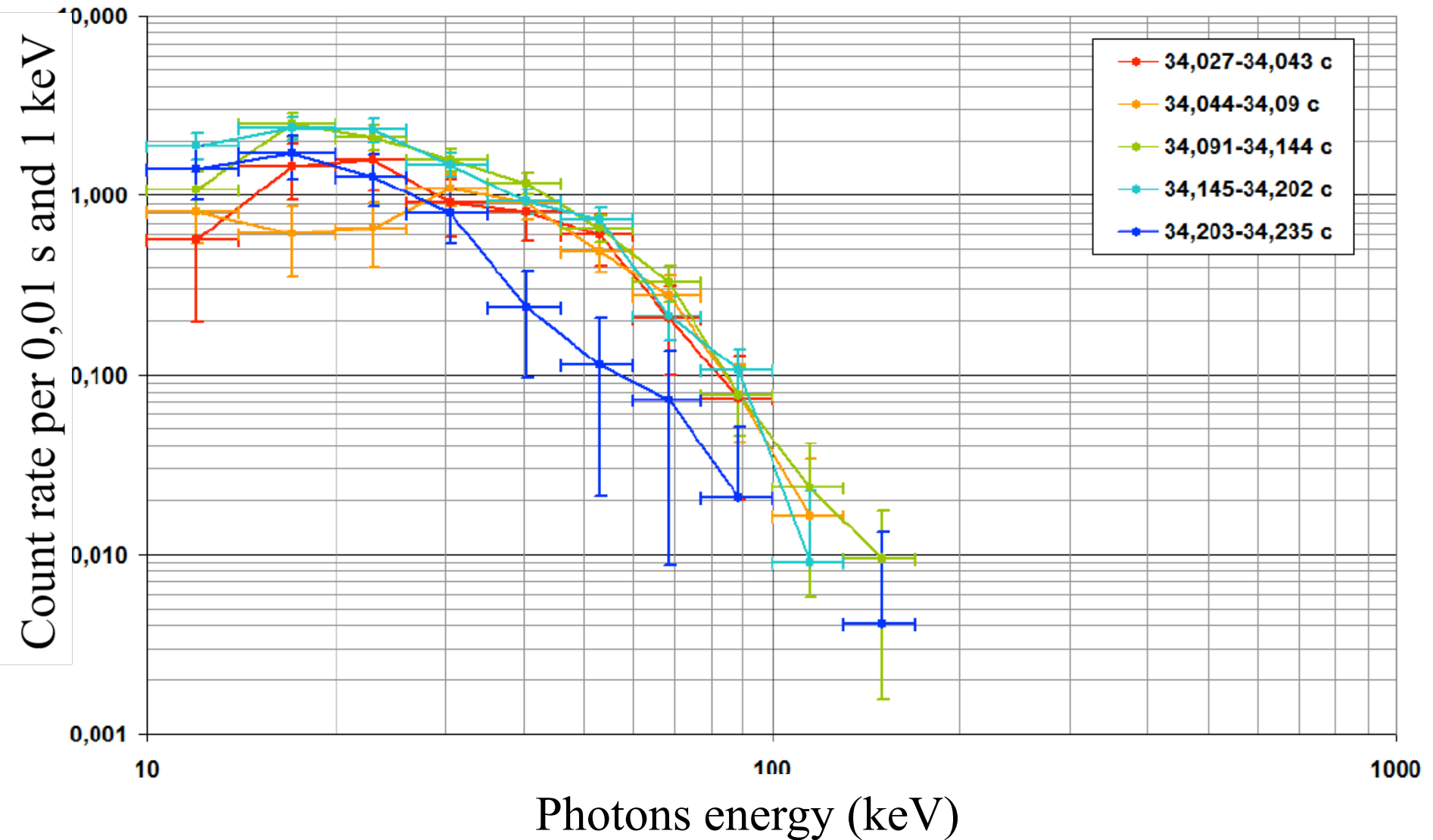
SGR 1935+2154 flare of 20.06.2016, 15:16:34 UT
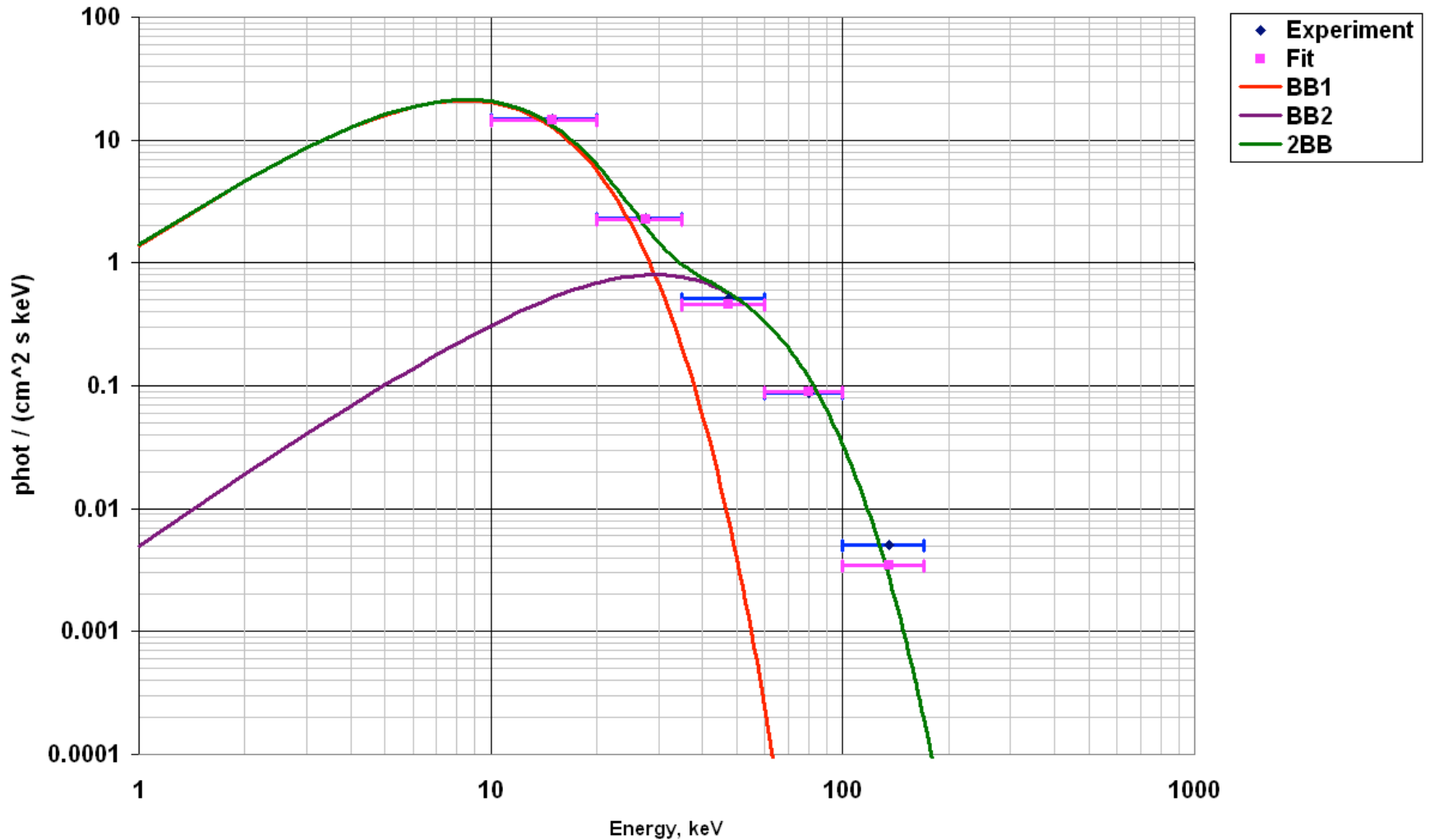
Fit by: $F(E) \sim A_1*(E^3/(\exp(E/kT_1)-1) + A_2*E^3/(\exp(E/kT_2)-1))$

with $kT_1 = 3$ кэВ, $kT_2 = 10.5$ кэВ, $A_1 = 1.3*10^{-2}$, $A_2 = 1.3*10^{-5}$
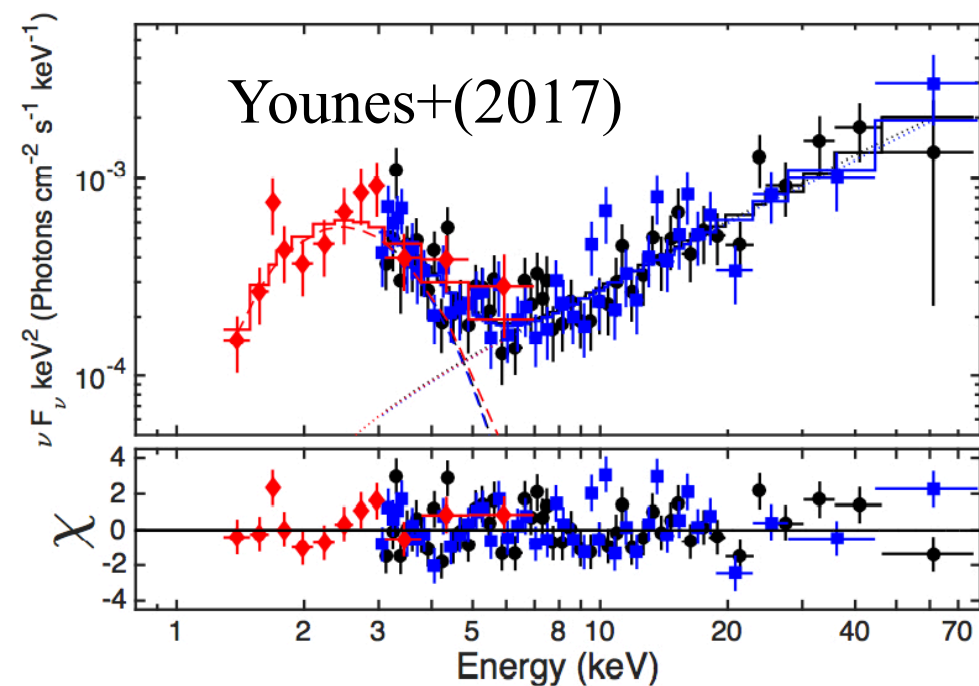
Younes+(2017)

Figure 5. *Upper panel.* Simultaneous broad-band *NuSTAR* and *Swift*-XRT spectra of SGR J1935+2154 taken on 2015 February 27, 5 days after the 2015 outburst onset. Dots, squares, and diamonds are the *NuSTAR* FPMA, FPMB, and *Swift*-XRT spectra, respectively. The solid lines represent the absorbed BB+PL best fit model in $\nu F\nu$ space, while the dashed and dotted lines represent the BB and PL components, respectively. *Lower panel.* Residuals of the best fit are shown in terms of standard deviation.
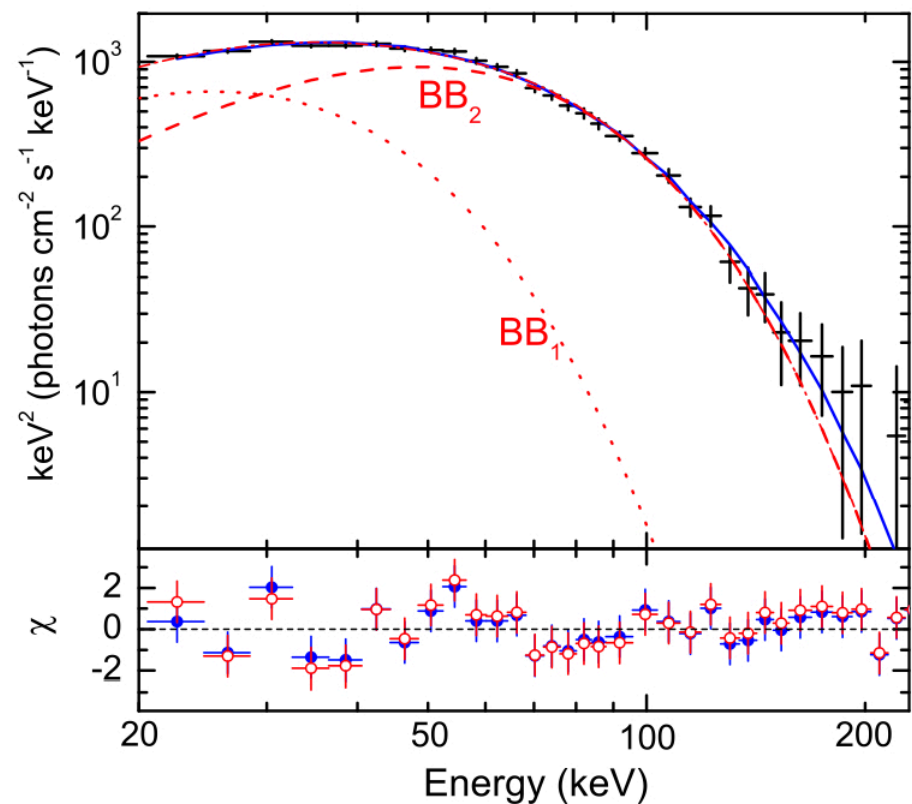
Figure 3. TI νF_ν spectrum of the flare: KW data (symbols); the CPL model (blue solid line); the 2BB model (red dash–dotted line) and its low-kT and high-kT components (red dotted and dashed lines, respectively). The bottom panel shows the fit residuals: filled and open symbols represent CPL and 2BB, respectively. [A color version of this figure is available in the online

Kozlova+(2016) for April 2015 flare

BDRG spectra provide BB $_1$ and BB $_2$ kT values quite similar to those of GBM, Konus-Wind and Swift BAT derived, typically:
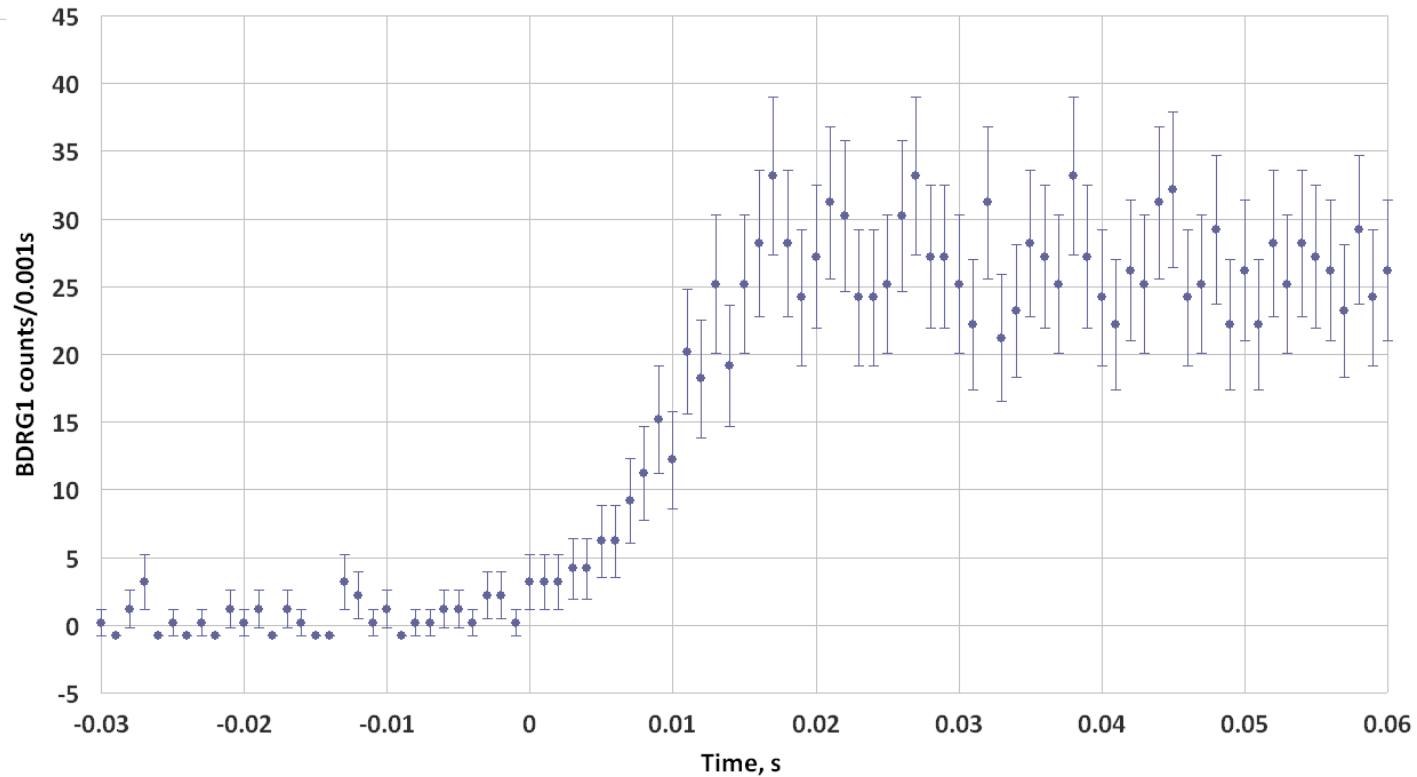$$kT_1 \sim 4 \text{ keV, and } kT_2 \sim 10 \text{ keV}$$
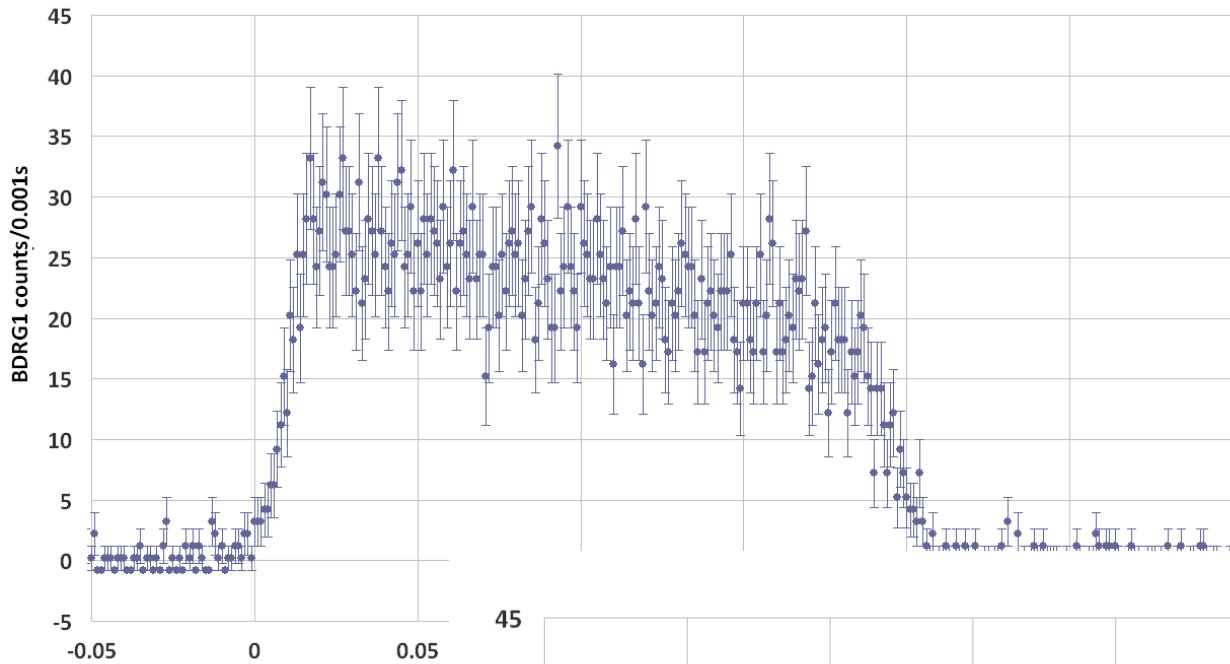
Light-curves for 2016.06.20 15:16:34 event by BDRG-1

Conclusions-1

1. Lomonosov registered 14 bursts of SGR 1935+1421 during June-July 2016;

2. Two of 14 bursts were self-triggered and provided good timing for two light-curves, especially for the June 20, 15:16:34 burst!

3. Clearly better statistic for magnetar burst photons, as well, as polarisation measurements for different energy channels will be helpful to put constrains on the emission mechanism!

Conclusions-2

4. Instruments with polarisation measurements capabilities are badly needed to help solving a few of the magnetar bursts problems!

Instruments under development:
XIPE->IXPE->XTP->EXTP + eASTROGAM-AMEGO +...?

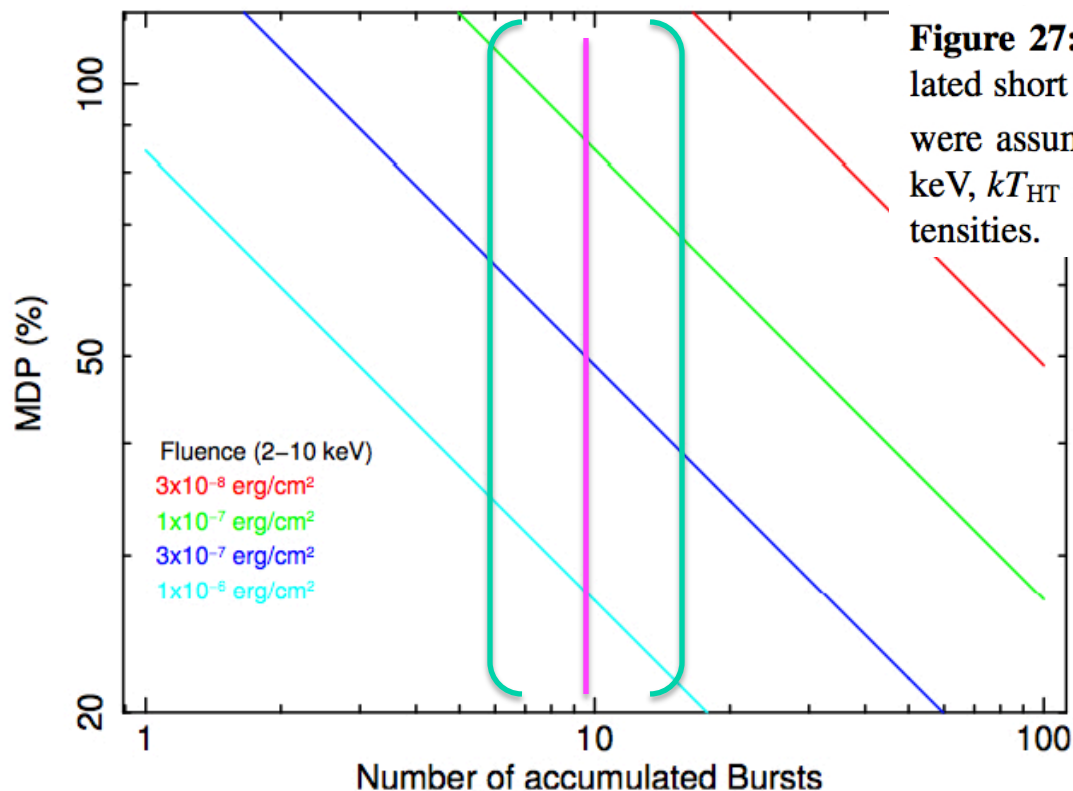Polarization detectability of SGR 1806–20 short burst by SGD

Figure 27: Simulated polarization detectability from accumulated short burst events by SGD. Spectrum from 1806-20 bursts were assuming two black body model: $\left(\frac{R_{HT}}{R_{LT}}\right)^2 = 0.01$, $kT_{LT} = 4$ keV, $kT_{HT} = 11$ keV (Nakagawa et al., 2007) in varied burst intensities.

Fluence (2–10 keV)
3×10^{-8} erg/cm^2
1×10^{-7} erg/cm^2
3×10^{-7} erg/cm^2
1×10^{-6} erg/cm^2

X-ray polarimetry with a Gas Pixel Detector (XIPE)

To efficiently image the track at energies typical of conventional telescopes IASF-Rome and INFN-Pisa developed the Gas Pixel detector. The tracks are imaged by using the charge.

A photon cross a Beryllium window and it is absorbed in the gas gap, the photoelectron produces a track. The track drifts toward the multiplication stage that is the GEM (Gas Electron Multiplier) which is a kapton foil metallized on both side and perforated by microscopic holes (30 um diameter, 50 um pitch) and it is then collected by the pixellated anode plane that is the upper layer of an ASIC chip.
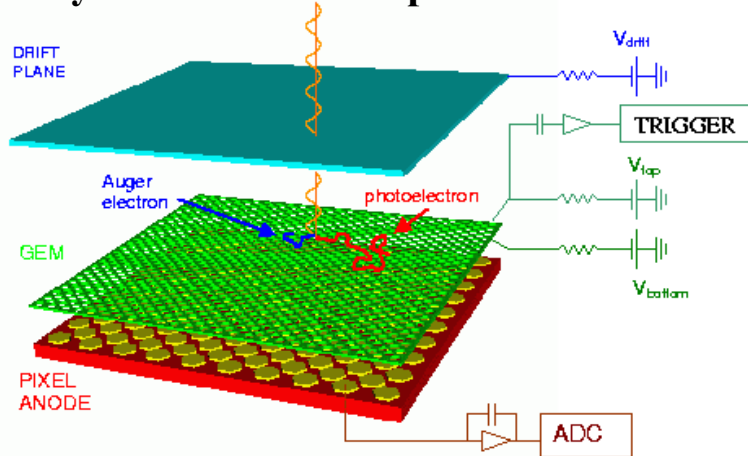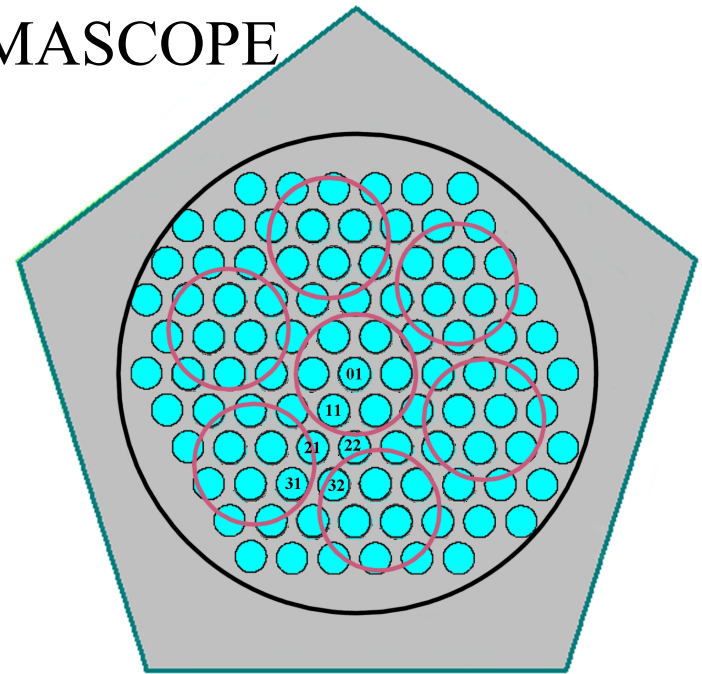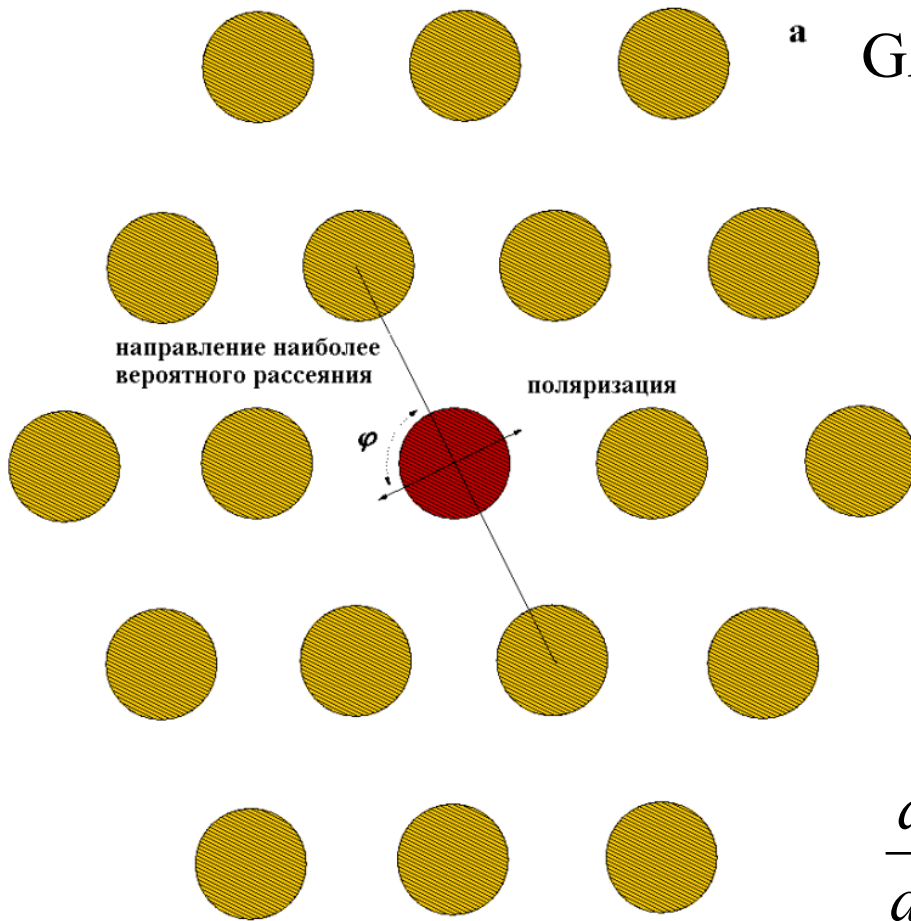
GEM electric field
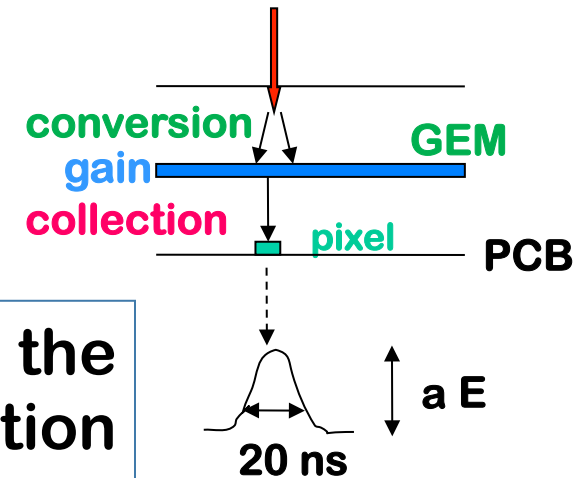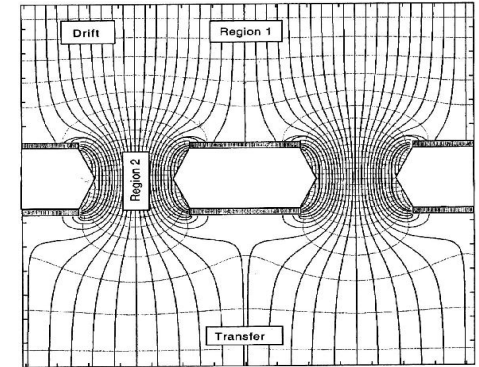
Costa et al., 2001, Bellazzini et al.2006, 2007

conversion
gain
collection
GEM
pixel
PCB

a E

20 ns

Polarization information is derived from the angular distribution of the emission direction of the tracks produced by the photoelectrons.
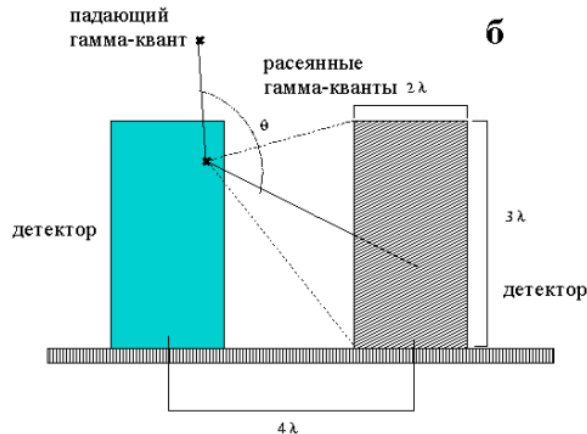The detector has a very good imaging capability.

GAMMASCOPE

$$\frac{dI}{d\varphi} = \frac{I}{2\pi}\left[1 - \mu P \cos^2\left(\varphi - \varphi_0\right)\right]$$

Compton polarimeter:
a – position-sensitive
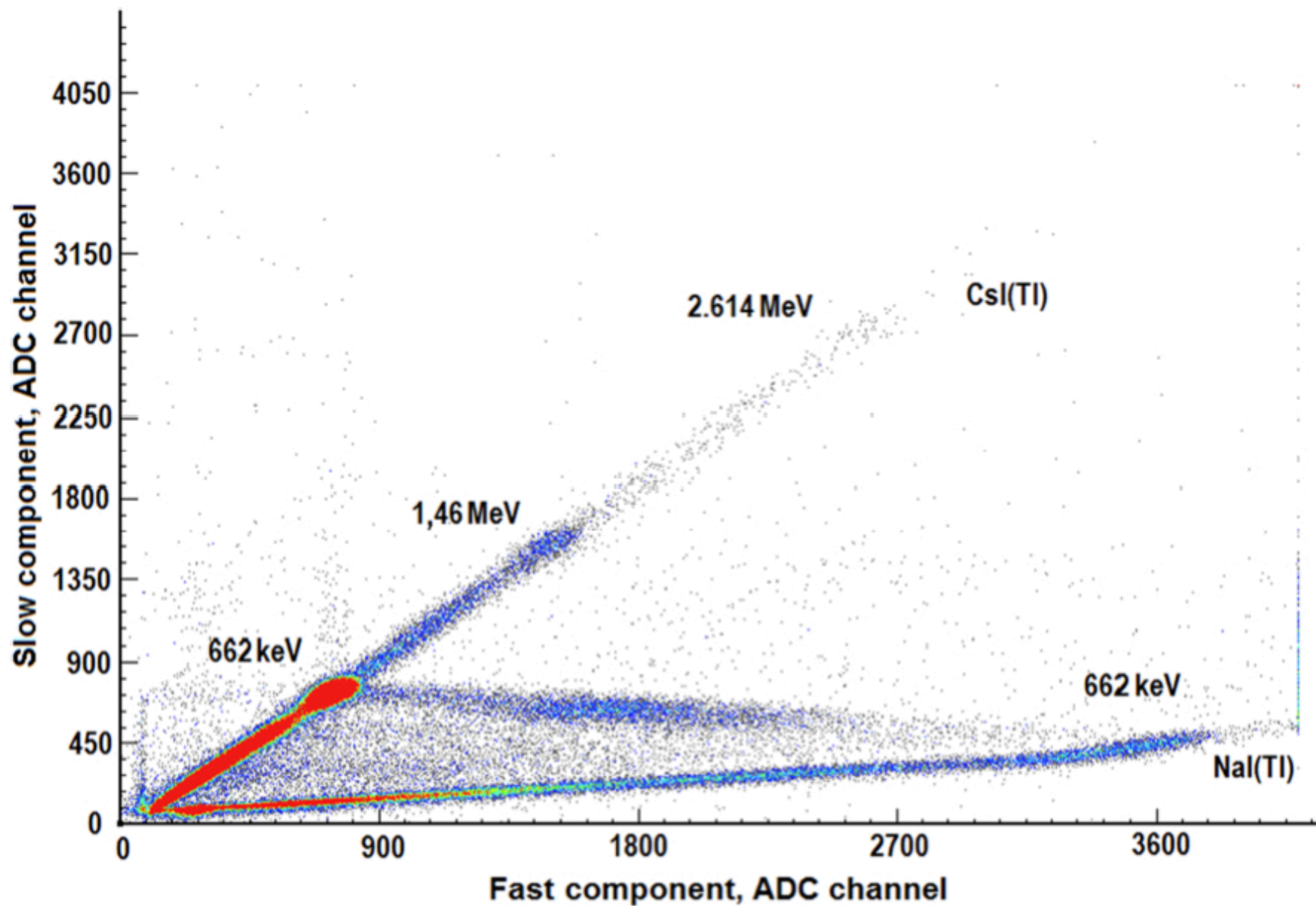**detector pixels, top view,**
b – PSD pixels, side view.

Svertilov et al. (2008)

THANK YOU!

Example of 2D-diagram plot of slow against fast components of a PMT pulse for ^{137}Cs

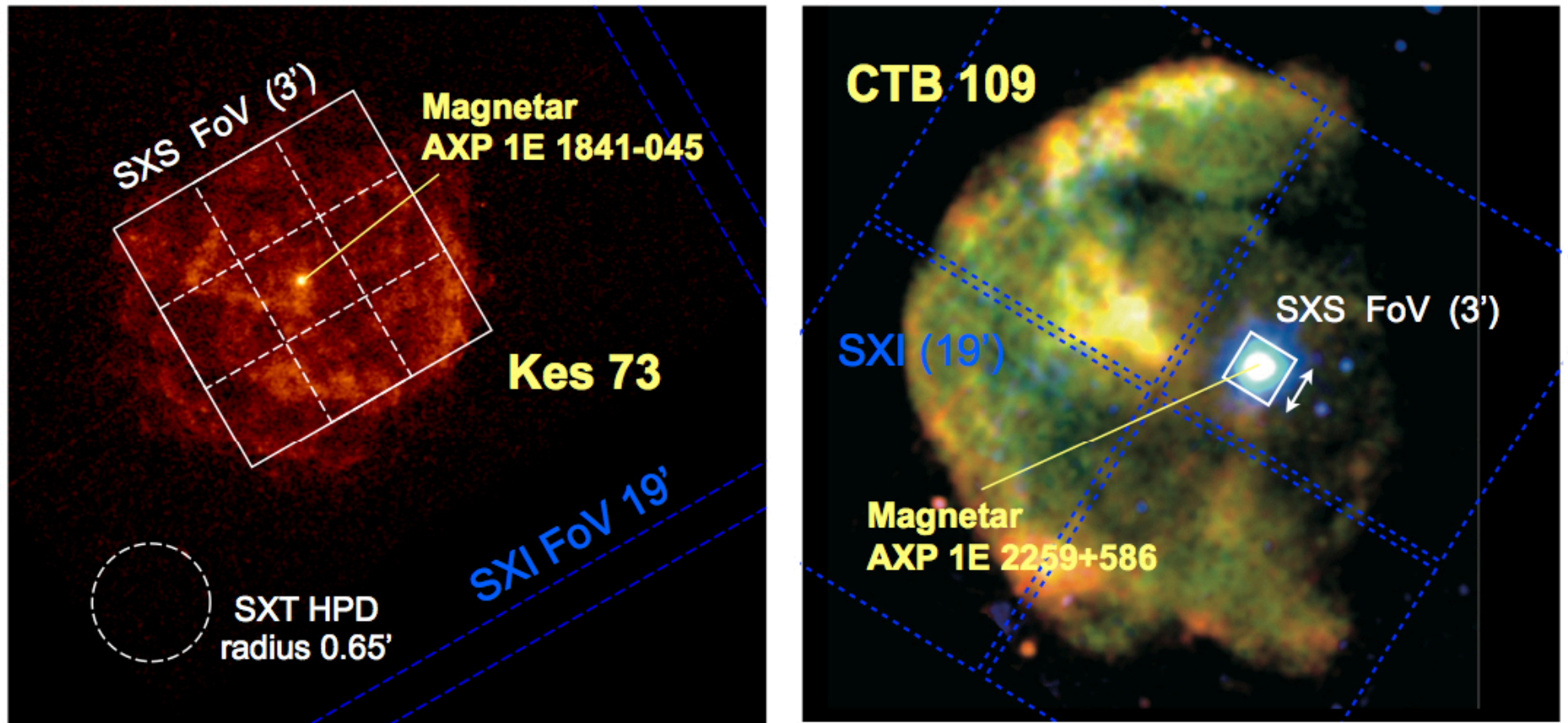# Magnetars and SNRs (from Astro-H WP (2014))

Figure 13: Bright magnetar SNRs: (left) The young SNR Kes 73 observed with *Chandra* with *ASTRO-H*'s SXS and SXI fields of view overlaid. The central source is the AXP 1E 1841–045. (right) The evolved SNR CTB 109 with *XMM-Newton* (Sasaki et al., 2004) with *ASTRO-H*'s SXS and SXI field of views. The central source is the AXP 1E 2259+586. The dim western half part of this SNR is covered by a giant molecular cloud.

Astro-H-WP: Kitamoto, Enoto, Safi-Harb et al., arXiv1412.1165v1